Journal of Constructional Steel Research 243 (2026) 110385

Contents lists available at ScienceDirect

Journal of Constructional Steel Research

journal homepage: www.elsevier.com/locate/jcsr

Hybrid-coupled walls with replaceable shear links: Experimental study of link-to-wall subsystems

Cristian Vulcu [a,*], Rajarshi Das [b], Rafaela Don [a], Benno Hoffmeister [a], Hervé Degée [c]

[a] Institute of Steel Construction, RWTH Aachen University, Mies-van-der-Rohe-Str. 1, 52074 Aachen, Germany
[b] SWECO Belgium, Herkenrodesingel 8B, bus 3.01, 3500 Hasselt, Belgium
[c] Construction Engineering Research Group, Hasselt University, Agoralaan Str., 3590 Diepenbeek, Belgium

ARTICLE INFO

Keywords:
Hybrid-coupled walls
Dissipative steel links
Bolted steel connections
Steel-concrete composite members
Experimental investigations
Seismic performance

ABSTRACT

Hybrid-coupled wall systems are a type of structural solutions that can be configured to achieve ductile seismic dissipation and enhanced post-earthquake repairability in buildings located in regions of moderate-high seismicity. In such systems, reinforced concrete or steel-concrete composite shear walls provide lateral stiffness and strength, while energy dissipation is concentrated in steel components designed to be replaceable after seismic events. This paper presents an experimental investigation on a novel hybrid-coupled wall system incorporating externally mounted, replaceable steel seismic links as dissipative components. The proposed configuration consists of a reinforced concrete or composite shear wall connected to adjacent steel columns through short steel links designed to yield in shear. The link-to-wall connection is detailed as moment-resisting to ensure force transfer and enforce the intended shear yielding mechanism in the link, while the simple link-to-column connection is configured to facilitate disassembly and replacement. A comprehensive experimental programme comprising monotonic and cyclic tests was conducted on subsystems to assess the overall response, the hysteretic behaviour, the damage localization and the connection performance. The results demonstrate stable hysteretic response with inelastic deformations effectively confined to the replaceable links, while the walls, boundary columns, and connection regions remain elastic. No degradation or unintended damage was observed outside the predefined dissipative components. The findings provide experimental evidence that hybrid-coupled walls with replaceable steel links can achieve controlled and predictable seismic response together with post-earthquake repairability, using a simplified dissipative strategy, and constitute a viable alternative for steel-concrete composite lateral load-resisting systems.

1. Introduction

1.1. Research background

In regions of moderate-to-high seismicity, lateral load-resisting systems are required to provide sufficient stiffness and strength while accommodating significant inelastic deformations in a controlled manner. In recent years, increasing emphasis has been placed on resilience and repairability [1], motivating research efforts to concentrate inelastic demand into predefined, replaceable components and to limit permanent damage to other structural elements. Reinforced concrete (RC) and steel-concrete composite shear walls are commonly employed to satisfy stiffness and strength demands in seismic context. Among wall solutions, coupled shear wall systems – composed of RC walls connected by RC coupling beams – were originally introduced by researchers [2–4] to enhance dissipation capacity compared to isolated walls. While effective in improving lateral resistance, these systems typically sustain extensive and permanent damage under cyclic lateral loading, particularly within the coupling beams and at the bases of the wall piers, where plastic hinges develop [5,6]. Subsequent developments sought to mitigate these drawbacks by replacing RC coupling beams with steel members, giving rise to hybrid-coupled wall (HCW) systems [7–11]. In this configuration, steel coupling beams are intended to act as dissipative structural fuses, aiming at improving post-earthquake repair. HCW systems are commonly implemented in combination with steel framing systems for gravity loads, resulting in coupled core walls or coupled perimeter wall arrangements [12]. Nevertheless, under cyclic lateral loading, often combined with axial force, the inelastic response of RC and steel-

* Corresponding author.
E-mail address: c.vulcu@stb.rwth-aachen.de (C. Vulcu).

https://doi.org/10.1016/j.jcsr.2026.110385
Received 21 January 2026; Received in revised form 11 March 2026; Accepted 31 March 2026
Available online 8 April 2026

concrete composite walls toward failure still involves concrete components and is characterised by distributed plastic mechanisms (e.g., concrete cracking and crushing, yielding of reinforcement, plastic hinging at the wall base) [13–16]. As a consequence, although adequate seismic behaviour can be achieved, the repair of such systems remains difficult and costly. To address these limitations, several design strategies have been developed to enhance seismic resilience, including approaches that avoid inelastic damage through rocking and protection of wall base regions, approaches that seek to localise inelastic demand within predefined components, as well as solutions combining both strategies.

One research direction has focused on rocking shear wall systems, in which uplift and rigid-body rotation – typically at the wall-foundation interface – is possible. Some of these systems employ unbonded post-tensioned (PT) tendons [17–19], which remain elastic during lateral loading and provide a restoring force upon unloading, resulting in re-centring and negligible residual displacements. Large-scale tests and analytical studies, including those carried out within the PRESSS research programme [20], demonstrated the feasibility of rocking wall systems and their application in engineering practice (buildings in New Zealand [21] and Chile [22]). However, due to their limited energy dissipation, purely rocking systems may experience increased displacement demands under strong ground motions [6]. To overcome this drawback, technical solutions were subsequently proposed, combining post-tensioning with additional dissipative components intended to yield in a ductile manner, while the PT tendons provide the restoring force responsible for re-centring. Dissipative components investigated in this context include mild steel bars [23], slit plates [24], friction devices [24–26], and different steel connectors [27] (e.g., O-connectors [28]). Although these combined solutions can achieve stable hysteretic behaviour with limited residual displacements, they are often challenging, relying on complex detailing and the need for a large number of dissipative components to be distributed throughout the structure in order to achieve the intended structural response. Another research direction has focused on composite steel plate shear walls combined with steel boundary structural elements. In these systems, thin steel plates act as the primary dissipative components, while precast concrete panels restrain buckling, enhance stiffness and strength, and reduce on-site construction effort compared to conventional shear walls [29]. Experimental studies further indicated that, under cyclic loading, damage in composite steel plate shear walls can be largely concentrated within the steel plate sandwiched between concrete panels, with limited cracking of the surrounding concrete [30]. However, it should be noted that composite steel plate shear walls require long bolted connections assembled on site, extensive welding between the steel plate and boundary frame, and relatively complex force transfer mechanisms between multiple components. Moreover, fracture of welded connections has been reported toward advanced loading stages [31], which could significantly complicate post-earthquake repair. As a result, some of the advantages of prefabrication may be offset, while repairability may be reduced.

Recent European research projects, notably INNO-HYCO [32], investigated HCW systems in which a single RC or composite wall is coupled to steel columns located on either side of the wall by means of embedded steel links incorporating replaceable segments defined through splice connections. Experimental and numerical studies demonstrated that steel links can provide adequate energy dissipation while offering the potential for replacement when employed in combination with RC and steel-concrete composite shear walls [33–35]. However, the development of unintended plastic deformations in the steel link-to-column connection region (i.e., yielding of web angles, ovalization of bolt holes in the link) was reported, compromising the intended plastic mechanism [36].

1.2. Normative perspective

Seismic design standards provide explicit provisions for steel-concrete composite walls, which are treated as lateral force-resisting structural systems with defined dissipation mechanisms and behaviour factors. In principle, composite shear walls and seismic links can be designed using existing, but separate provisions. In current standards, however, their interaction is realised predominantly through RC or steel coupling beams. In the European framework, EN 1998–1 [37] addresses composite shear walls through a system-based classification comprising three structural types: Type 1 - steel or composite frames with infill walls; Type 2 - concrete walls with encased steel sections interacting with a concrete structure; and Type 3 – RC or composite walls coupled by steel or RC beams. For all wall system types, energy dissipation is expected to occur primarily within the steel components of the walls themselves (i.e., vertical reinforcement and/or encased steel profiles). For Type 3 systems, additional energy dissipation is explicitly permitted in the coupling beams. Behaviour factors are provided for each system and for ductility classes DCM and DCH, and the design philosophy mandates that non-dissipative components and the connections of dissipative parts possess sufficient overstrength to enable stable cyclic yielding in the intended dissipative regions. Provisions for connections located in dissipative zones further aim to limit excessive stress concentrations and to limit damage to predefined steel elements. Recent draft developments in prEN 1998-1-2 [38] retain the structural system types for composite steel-concrete buildings while introducing a clearer performance differentiation through ductility classes (DC) DC2 and DC3. For composite wall systems, the draft standard provides updated behaviour factors, explicit limits on the seismic action index (in prEN 1998-1-1 [39]), and interstorey drift limits at the Significant Damage limit state. Explicit provisions for steel links are introduced in dedicated sections of European seismic codes and in parallel draft documents. prEN 1998-1-2 [38] and prEN 1998-1-101 [40] define seismic links as dissipative elements intended to undergo plastic deformation in bending and/or shear, and impose explicit rotation capacity requirements. For short links designed for DC2 and DC3, a plastic rotation capacity of 0.08 rad is required, whereas for long links the required plastic rotation capacity is 0.02 rad. In both cases, the associated strength degradation is restricted to a maximum reduction of 20% of the peak shear resistance at the prescribed rotation capacity. The rotation angle θ_p, measured between the seismic link and the adjoining structural element is also explicitly limited for short links (i.e., the plastic rotation demand should be less than 0.08 rad). While these provisions provide clear quantitative performance targets for seismic links, they are formulated independently of the composite wall system classification, leaving unresolved how such links should be consistently integrated into composite shear wall design under Eurocode 8.

In U.S. practice, the design of RC and steel-concrete composite shear walls is governed by ACI 318 [41], while AISC 341 [42] classifies composite shear wall systems as ordinary or special, and defines the associated seismic requirements for steel components and global system behaviour. For composite special shear walls, AISC 341 [42] prescribes explicit yielding hierarchies (i.e., coupling beams shall yield prior to the wall base), deformation demands and overstrength requirements. The design of coupling elements is linked to the provisions for seismic links, including prescribed rotation limits, providing a good basis for performance-based seismic design.

1.3. Research scope and methodology

Against this background, numerous solutions have been proposed to promote damage control and improve post-earthquake repairability. However, many of these solutions rely on complex detailing and multiple interacting components which complicate their practical implementation. As a result, achieving damage control, simplicity of the structural solution and repairability was an open challenge. The present

study investigates the behaviour of novel HCW systems in which RC or steel-concrete composite shear walls are connected to steel side (or boundary) columns through externally mounted, replaceable steel seismic links. Unlike other solutions, the proposed configuration employs a single wall, with energy dissipation occurring through steel seismic links. Designed as dissipative components, the short links yield in shear while the walls, the boundary columns, and the connections are intended to remain elastic. In this configuration, the side columns primarily resist alternating axial tension and compression. By approximating a pinned support, the link-to-column connection facilitates shear transfer while attracting only a negligible bending moment. A steel filler plate interposed between the link's end-plate and the column flange provides clearance to allow replacement of the damaged link. The link-to-wall connection transfers both shear force and bending moment.

Conducted at RWTH Aachen University as part of the RFCS-funded HYCAD project [43] the experimental programme presented herein focuses on the behaviour of the HCW superstructure. This work builds upon previous developments, notably the INNO-HYCO project [32], advancing the concept through the integration of prefabricated elements and redesigned link connections optimized for damage control and repair. The research approach consisted of technical solution development of two HCW configurations (see Section 2) and their experimental investigation under monotonic and cyclic loading conducted in accordance with ECCS 1986 [44] and EN 15129 [45]. For each tested configuration, the wall and boundary column were kept, while the shear links were replaced. The experimental investigations allowed to evaluate the monotonic and cyclic performance. In particular, the following response parameters were established: monotonic and cyclic shear force–deformation curves, failure mode, behaviour of the components, and mechanical characteristics (stiffness, shear capacity, rotation capacity, hysteretic behaviour). The plastic rotation capacity was evaluated against the prEN 1998-1-2 [38] performance requirement for seismic links in frames with eccentric bracings of length $1.6 \bullet M_{p,link}/V_{p,link}$ for ductility classes DC2 and DC3.

While the resulting HCW solutions are compatible with both fixed and pinned wall bases – configurations investigated by other project partners - the present contribution focuses exclusively on the superstructure performance (i.e., subsystems composed of a side column, shear link and RC/composite wall). The overarching aim of the study is to develop HCW solutions that combine adequate and predictable seismic behaviour with repairability. To this end, the investigation is guided by the following objectives:

1. The link acts as the primary dissipative fuse and accommodates the imposed shear demand.
2. The link-to-wall connection is non-dissipative and sustains combined shear and bending moment.
3. The link-to-column connection is non-dissipative and primarily transfers shear forces.
4. The wall is non-dissipative.
5. The link is designed to be disassembled after a seismic event.

Note: Objective (4) does not include the base of the wall, which might be a dissipative zone in case of walls fixed into the foundation. Referring to objective (5), it should be noted that, depending on a variety of factors, such as the overall building structural system, the seismic intensity, residual drifts, and permanent deformations, which are beyond the scope of the present study - the removal of the yielded links may be followed by the installation of new shear links.

This work offers experimental insights into the behaviour of HCW systems with replaceable steel links. The results presented herein support the development of repairable seismic solutions, enhancing the structural resilience of steel-concrete composite buildings in moderate-to-high seismic regions.

2. Experimental programme

2.1. Test specimens

To satisfy the stated objectives, several technical solutions were redesigned. First, at the link-to-wall connection, embedded steel profiles which hinder rebar placement, were replaced with post-tensioned connecting devices installed within ducts cast into the wall. This solution simplifies reinforcement placement and allows loosening or removal of the post-tensioned connecting devices, allowing damaged links to be disassembled after an earthquake. Second, the link-to-column connection was simplified. A flush end-plate connection was used to facilitate on-site assembly and to promote plastic hinge formation exclusively in the link. By concentrating inelastic demand in the intended fuse (shear link), the HCW configurations can achieve predictable seismic behaviour and remain compatible with post-event disassembly. Third, prefabrication was introduced through the use of precast double-slab wall panels subsequently infilled with on-site concrete. These panels reduce on-site wet works and eliminate the need for formwork.

Two HCW configurations were developed (Fig. 1 and Table 1): configuration 1 (*HCW_C-1*) and configuration 2 (*HCW_C-2*). Each configuration consisted of a short steel link connected on one side to the wall through a moment–shear connection and on the other side to a steel column through a hinged shear connection. The two configurations differed mainly in the following aspects:

- Fabrication method of the wall:
  - o *HCW_C-1*: cast in-situ;
  - o *HCW_C-2*: precast double-slab panels with on-site concrete infill;
- Link-to-wall connection:
  - o *HCW_C-1*: long post-tensioned connecting devices with embedded steel plates;
  - o *HCW_C-2*: shorter connecting devices combined with encasing profiles and a built-in steel box (either a rectangular hollow section (RHS) or a built-up steel profile).

Fig. 2 shows the bolt arrangements adopted for the link connections in the two investigated configurations. Specifically, the figure shows the link-to-wall connection details for *HCW_C-1* (Fig. 2a) and *HCW_C-2* (Fig. 2b). In addition, the bolt arrangement for the link-to-column connection, which is common to both configurations, is also presented (Fig. 2c). Fig. 3 illustrates the position of the investigated subassemblies within a building structure equipped with HCWs.

With regard to the design methodology adopted to define the specimen dimensions and connection arrangement used in the tests, it should be emphasised that a comprehensive design framework - encompassing numerical modelling, calibration, parametric investigations, stiffness and strength characterization, and the formulation of a step-by-step design procedure - is currently being finalised in a companion paper. Nevertheless, the principal design considerations underlying the tested specimens are summarized below.

Wall and side column design. The cross-sections of the RC wall and the side steel column were not determined through capacity design starting from the shear link strength. Instead, both elements were first defined via structural analysis and design of a representative case-study building (Fig. 3). Subsequently, representative segments of the wall and column were isolated for subsystem testing. For the wall segment, verification ensured that local crushing of the concrete would not occur due to the combined effects of pretension forces in the threaded rods and compressive stresses induced by bending in the shear link. Similarly, for the side column segment, potential local failure mechanisms, such as bearing at the bolt holes, flange or web local deformation, were explicitly checked.

Capacity design philosophy. Capacity design principles were explicitly applied to the link-to-wall and link-to-column connections. The shear link was designated as the sole dissipative component,

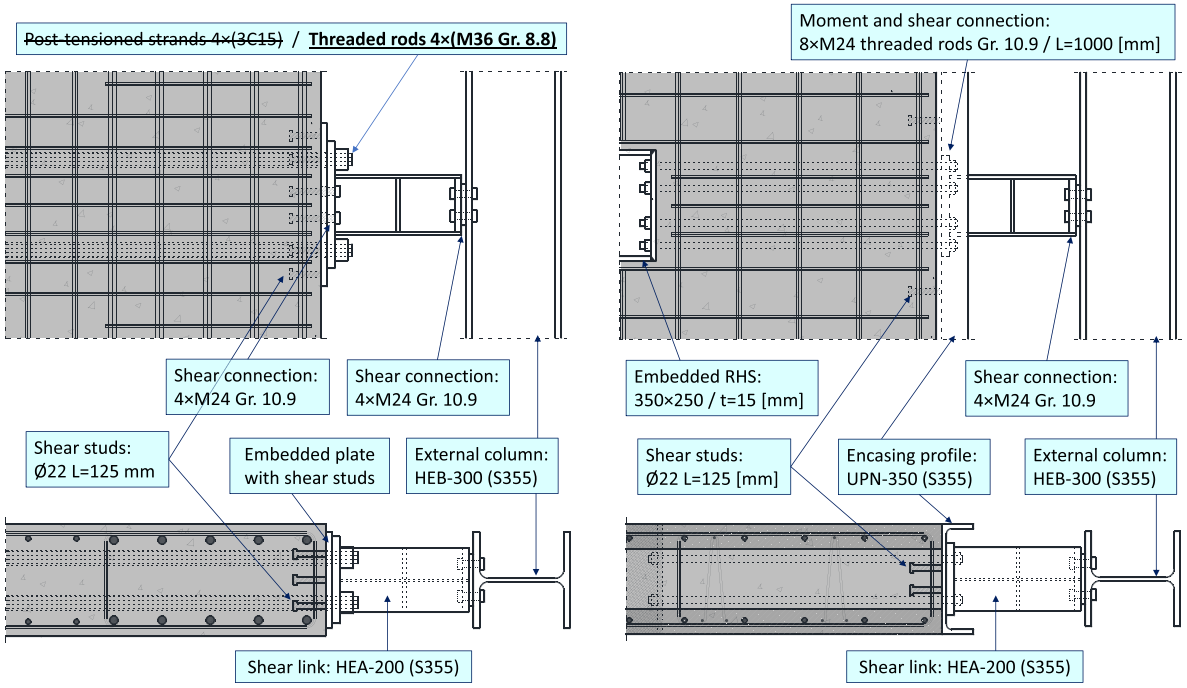

Fig. 1. Investigated HCW solutions, including connections: (a) *HCW_C-1* and (b) *HCW_C-2*.

Table 1
Comprehensive overview of the investigated HCW specimens.

	Configuration HCW_C-1 (Fig. 1a)		*Configuration HCW_C-2* (Fig. 1b)	
	Materials	Cross-sections & details	Materials	Cross-sections & details
Link	S355	HEA 200 Length e = 400 mm Ratio e/(M_{pl}/V_{pl}) = 0.8 Web stiffeners t_s = 10 mm	S355	HEA 200 Length e = 400 mm Ratio e/(M_{pl}/V_{pl}) = 0.8 Web stiffeners t_s = 10 mm
Wall	C35/45 B450 rebars	Cast in-situ wall 2000 × 2000 × 350 mm	C35/45 B450 rebars	Precast double-slab wall (+ infill) 2000 × 2000 × 350 mm
Column	S355	HEB 300	S355	HEB 300
Link-column connection	Flush end-plate connection (Fig. 2c): 4 × M24, Gr. 10.9 + filler plate		Flush end-plate connection (Fig. 2c): 4 × M24, Gr. 10.9 + filler plate	
Link-wall connection	Wall side: Embedded steel plate (t_{pl} = 20 mm) with 10 headed studs (D = 22 mm, L = 125 mm) Within wall: – Link side: Steel end-plate: t_{ep} = 25 mm Post-tensioned threaded rods (for bending moment transfer): 4 × M36, Gr. 8.8 High-strength bolts (for shear force transfer): 4 × M24, Gr. 10.9		Wall side: Encasing UPN 350 profile with 12 headed studs (D = 22 mm, L = 125 mm) Within wall: Built-in RHS 350 × 230 × 15 mm Link side: Steel end-plate: t_{ep} = 25 mm Post-tensioned threaded rods (for bending moment and shear force transfer): 8 × M24, Gr. 10.9	

whereas the connections were designed as non-dissipative elements intended to remain elastic under the maximum expected link force, including strain-hardening effects. Accordingly, the connections were proportioned considering the overstrength of the fully yielded and strain-hardened shear link. The detailed formulation of the adopted overstrength factors and corresponding design equations will be presented in the forthcoming companion paper.

The experimental programme presented herein focuses specifically on the seismic response of the steel link and two alternative link-to-wall connection solutions. The following subsections provide a detailed description of the investigated HCW configurations.

2.1.1. *Configuration 1 (HCW_C-1)*

Configuration 1 (*HCW_C-1*) consisted of a steel link, a cast in-situ reinforced concrete (RC) wall and an external steel column. The link was 400 mm long. The connection between the link and end-plates was realised using full-penetration welds and root re-welding at the flanges, and with fillet welds at the web. The RC wall measured 2000 × 2000 × 350 mm (height × width × thickness).

The link-to-wall connection was intended to transfer both shear and bending while allowing for link disassembly. On the wall side, the connection incorporated an embedded steel plate equipped with 10 shear studs; on the link side, it used an extended end-plate. These two plates were joined through post-tensioned connecting devices. The original connecting devices comprised 2 rows of 3C15 post-tensioned tendons (f_y > 1770 N/mm^2) arranged above and below the link to transfer bending moments. Shear transfer was achieved through 4 × M24 high-strength bolts positioned between the link flanges, since shear cannot be carried by post-tensioned tendons. However, this solution had to be revised due to the unavailability of the contractor responsible for the installation and post-tensioning of the tendons. As no replacement was available on short notice, the tendons were substituted with 4 × M36 Gr. 8.8 threaded rods (Fig. 1a, Table 1), while retaining the post-tensioning concept. This alternative was adopted because it appeared feasible to implement with less specialised equipment and, potentially, without hydraulic jacks.

The link-to-column connection primarily transferred shear. It consisted of a flush end-plate, 4 × M24 high-strength bolts and a filler steel plate inserted between the end-plate and the column flange to facilitate

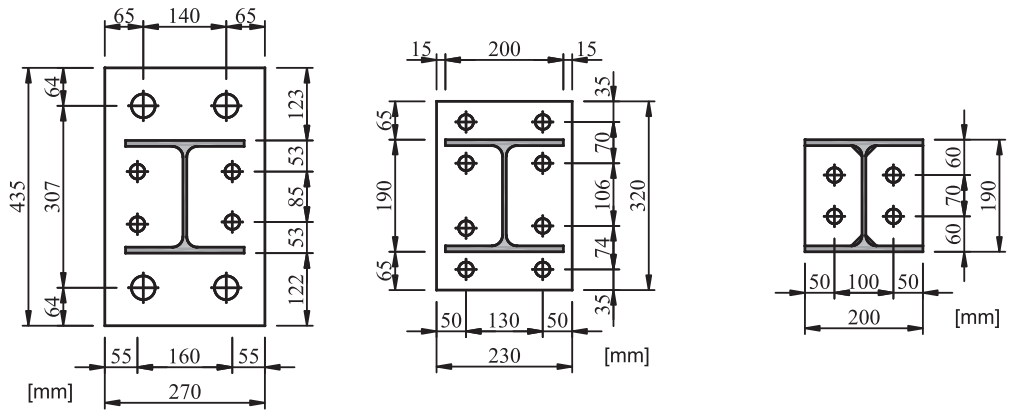

(a) detail for *HCW_C-1* (b) detail for *HCW_C-2* (c) detail for both HCW configurations

Fig. 2. Bolt arrangements for the link-to-wall connection in (a) *HCW_C-1* and (b) *HCW_C-2*, and for the link-to-column connection in both configurations (c).

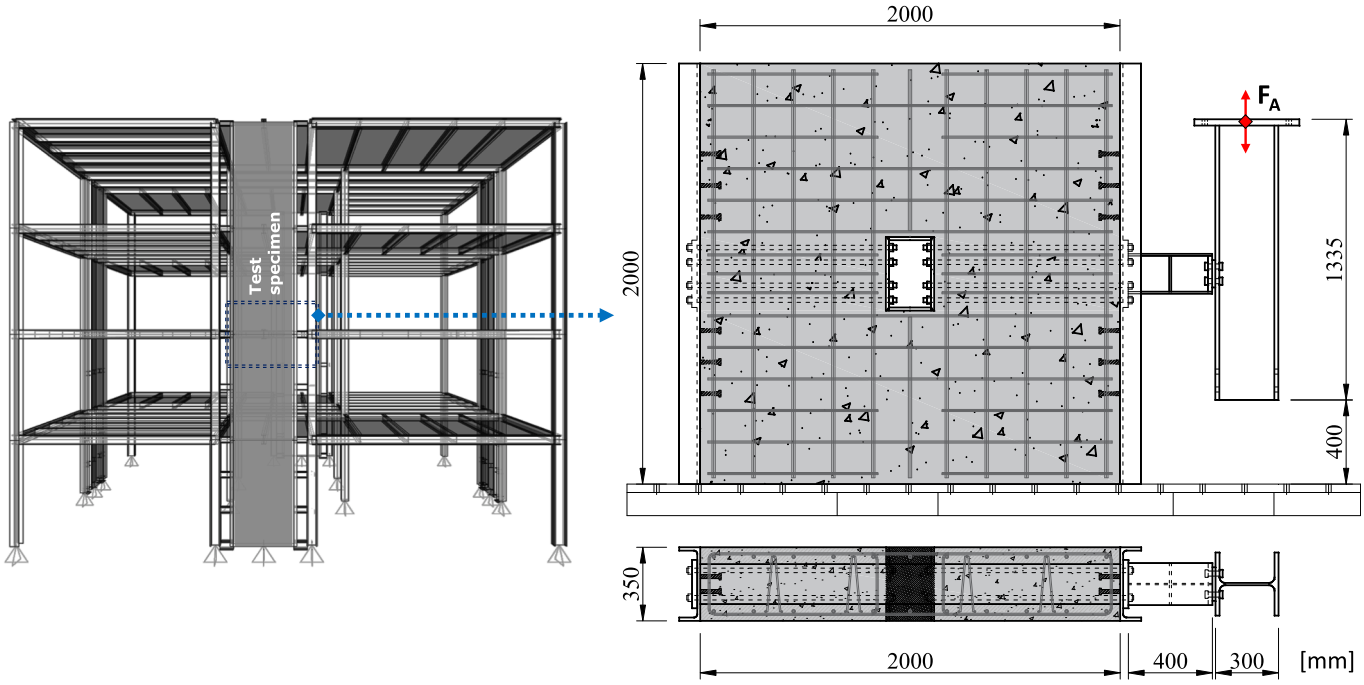

Fig. 3. Conceptual representation of a building structure equipped with HCWs and an isolated HCW subassembly showing overall dimensions.

the disassembly of the yielded link.

2.1.2. Configuration 2 (HCW_C-2)

Configuration 2 (*HCW_C-2*) employed a different wall construction method and link-to-wall connection. Specifically, *HCW_C-2* comprised a steel link, a steel-concrete composite wall formed by precast double-slab panels with on-site concrete infill and an external steel column. As in *HCW_C-1*, the link was 400 mm long and welded to the end-plates using full-penetration welds with root re-welding at the flanges and fillet welds at the web. The composite wall had the same dimensions as the RC wall, (2000 × 2000 × 350 mm).

The link-to-wall connection transferred both bending and shear while allowing for link disassembly. In contrast to the previous configuration, *HCW_C-2* employed a post-tensioned connection composed of 8 × M24 threaded rods in combination with encasing UPN steel profiles and a steel box cast into the wall (RHS 350 × 230 × 15 mm). The centrally positioned box allowed the use of shorter threaded rods (length of 1000 mm). This arrangement aimed to improve the reinforcement detailing around the link-to-wall connection and to eliminate the need for formwork. As in *HCW_C-1*, the link-to-wall connection relied on post-tensioning (Fig. 1b, Table 1).

The link-to-column connection (Fig. 1 and Fig. 2c) in *HCW_C-2* was identical to that used in *HCW_C-1*.

2.2. Loading protocols, test setup and instrumentation

Each HCW configuration was tested under three loading protocols: a monotonic test, a cyclic test following ECCS 1986 [44] and a cyclic test conducted in accordance with EN 15129 [45]. The full test matrix is summarized in Table 2 while the specimen labelling scheme is explained in Fig. 4.

The experimental setup used for both tested configurations is shown in Fig. 5. Specifically, the wall corresponding to each HCW subsystem was placed directly on the platform of the test rig. The lower part of the side column was equipped with two thick steel plates, which were in contact with a steel profile anchored to the platform. Polytetrafluoroethylene (PTFE) layers were used to minimize friction between the plates and the profile, and to ensure that the column could move

Table 2
Experimental programme.

Configuration	Label	Wall description	Loading	No. tests
Config. 1	*HCW_C-1*	Cast in-situ RC wall with embedded steel plates	Monotonic Cyclic	1 2
Config. 2	*HCW_C-2*	Composite wall with precast double-slab panels, infill and encasing steel profiles	Monotonic Cyclic	1 2

vertically as intended. As a result, the column was subjected solely to axial tension and compression. Although PTFE layers were employed to isolate the behaviour of the link-to-HCW subsystem, comparable boundary conditions can be achieved also in practical building structures, where column bases are not required to be fully fixed, since their primary function is to transfer axial forces (tension and compression) to the foundation. Therefore, the experimental findings regarding link behaviour remain directly applicable to real building scenarios.

Out-of-plane stability was provided by a restraining system consisting of four vertical steel profiles positioned on either side of the wall and two horizontal steel profiles placed on top of the wall. These elements were connected to each other and to the platform, preventing both lateral and vertical movement of the wall throughout the tests. The loading was applied using a 1000-kN-capacity hydraulic actuator attached to the top of the column, with the actuator displacement controlling the imposed deformation.

The instrumentation for specimens *HCW_C-1* and *HCW_C-2* is shown in Fig. 6 and Fig. 7, respectively. The sensor arrangements were designed to capture relevant global and local responses of the HCW subsystems. Specifically, the objective was to measure the response of the shear link as well as the link-to-column and link-to-wall connections.

For the *HCW_C-1* specimens, the following quantities were recorded:

- Applied load: actuator force and displacement.
- Vertical displacements: of the column and of the link.
- Relative displacements at the connections:
  o between the column and the link,

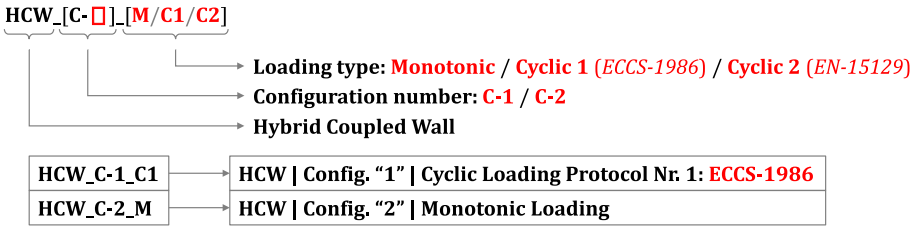

Fig. 4. Labelling of specimens.

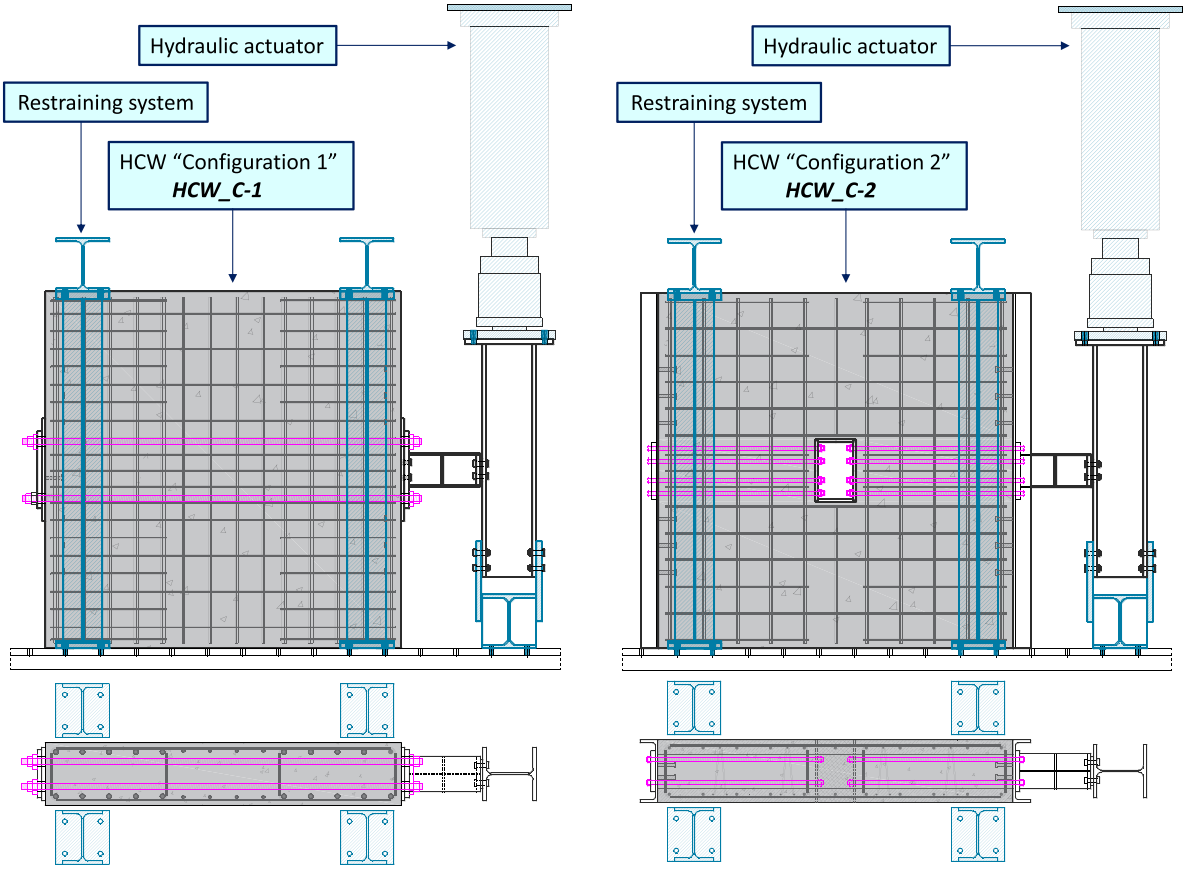

(a) *HCW_C-1* (b) *HCW_C-2*

Fig. 5. Test setup for configuration *HCW_C-1* and *HCW_C-2*.

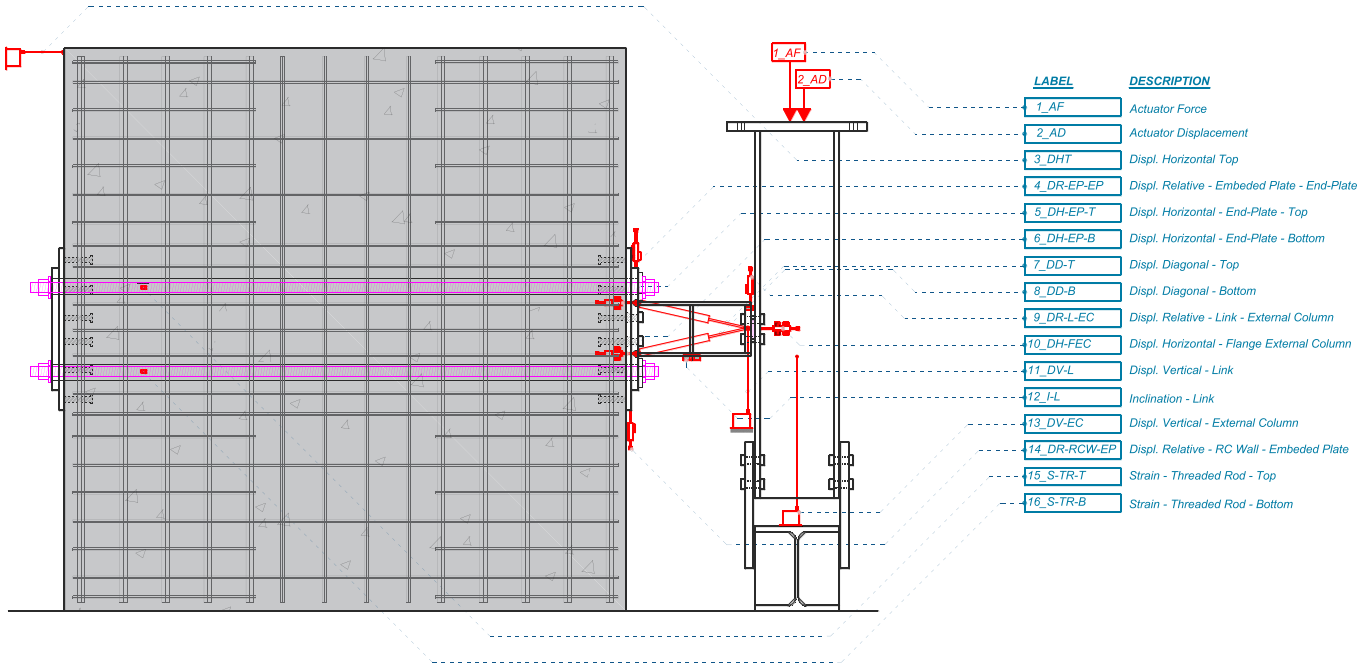

Fig. 6. Instrumentation for configuration *HCW_C-1*.

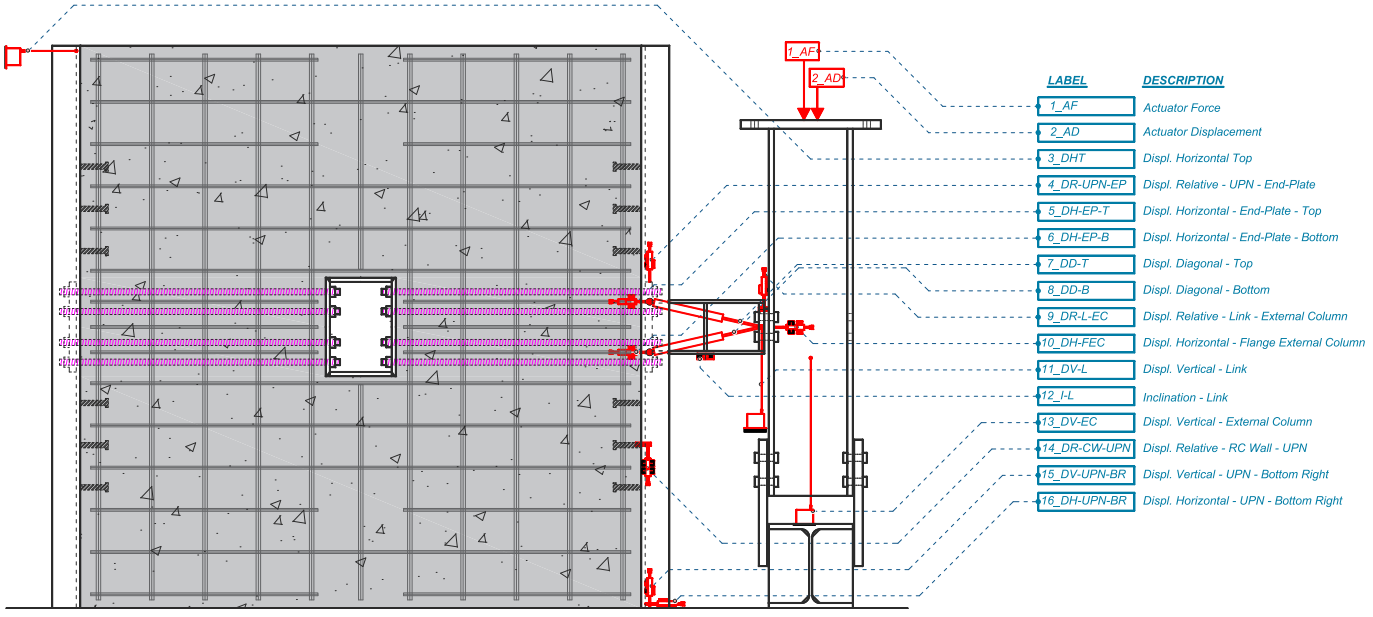

Fig. 7. Instrumentation for configuration *HCW_C-2*.

  - o between the embedded plate and the end-plate, and
  - o between the embedded plate and the RC wall.
- Link deformation: inclination and shear deformation.
- Deformation of the link-to-wall connection: end-plate deformation under tension and compression.
- Wall displacement: horizontal displacement at the top of the RC wall.
- Post-tensioned system: strain in the threaded rods prior and during testing, to monitor the variation of the transferred force.

For the *HCW_C-2* specimens, the same measurements were carried out with the following modifications:

- Relative displacements at the connections:
  - o between the column and the link,
  - o between the encasing UPN profile and the end-plate, and
  - o between the encasing UPN profile and the wall.
- Strains in the post-tensioned threaded rods were not measured in this case.

2.3. Material properties

Material properties were determined through coupon testing. Steel coupons were machined from the flange and web of the same profile (HEA 200, S355 structural steel) that was used to fabricate the shear links. The corresponding engineering stress–strain curves are presented in Fig. 8. Concrete samples were extracted from the C35/45 wall infill

and tested in compression and tension. No additional material samples were taken, as the remaining steel components (external column, end-plate, UPN profile, and rebars) did not experience plastic deformation during the tests and therefore did not require further characterization. The results of the material tests are summarized in Table 3 and Table 4.

2.4. Fabrication of the specimens

The step-by-step fabrication and assembly procedure for the *HCW_C-1* specimens is outlined below. Fig. 9 illustrates the procedure and provides visual clarification of the steps.

1. Component identification and geometry measurement.
2. Fabrication of the wall:
   - o Assembly of formwork;
   - o Arrangement of the reinforcement and positioning of the embedded plates (Fig. 9a);
   - o Positioning of the plastic ducts, to be used for the insertion of the threaded rods (Fig. 9b);
   - o Casting of the concrete (Fig. 9c-d);
   - o Removal of the formwork after concrete hardening (Fig. 9e).
3. Assembly of the test setup, including the *HCW_C-1* specimen.
4. Insertion of the threaded rods into the RC wall after machining and instrumentation with strain gauges (Fig. 9f).
5. Instrumentation of the entire specimen and post-tensioning of the threaded rods using a pneumatic torque wrench (Fig. 9g).

Related to point (3) from the above list, as well as to Fig. 1a, two separate sets of 4 × M24 bolts were used. One set connected the shear link to the external steel column, and was installed with the filler plate and hand-tightened. The second set transferred shear force to the reinforced concrete (RC) wall; to prevent participation to bending resistance, the nuts were placed in hexagonal holes of the embedded plate (see Fig. 9a), and the bolts were then inserted and hand-tightened after positioning the link.

The fabrication and assembly of the *HCW_C-2* specimens followed the sequence outlined below. Fig. 10 illustrates the procedure and provides visual clarification of the steps.

1. Component identification and geometry measurement.
2. Fabrication of the composite wall:
   - o Prefabrication and delivery of the double-slab wall panels and steel members (Fig. 10a);
   - o Positioning of the built-in RHS profile into the precast double-slab wall (Fig. 10b);
   - o Insertion of the threaded rods, including plastic ducts (Fig. 10b);
   - o Positioning of the encasing UPN profiles and tightening of the threaded rods (Fig. 10c);
   - o On-site concrete infill casting between the double-slab panels and concrete hardening (Fig. 10d-f).
3. Assembly of the test setup, including positioning of *HCW_C-2* specimen (Fig. 10f).
4. Instrumentation of the specimen.

Table 3
Average material properties of the steel coupons (HEA 200, S355).

Material properties	HEA 200 flange	HEA 200 web
Yield strength: f_y	396 N/mm^2	429 N/mm^2
Ultimate strength: f_u	538 N/mm^2	552 N/mm^2
Ratio f_u / f_y	1.35	1.28
Elongation at maximum force: A_g	16.7%	15.5%
Elongation at fracture: A	32.6%	28.9%
Elastic modulus E	196,647 N/mm^2	206,670 N/mm^2

Table 4
Material properties of the concrete samples (C35/C45).

Material properties	At 7 days (on cubes)	At 10 days (on cylinders)	At 100 days (on cubes)
Compressive strength f_{ck}	42.1 N/mm^2	38.1 N/mm^2	47.7 N/mm^2
Tensile strength f_{tk}	–	2.9 N/mm^2	–
Elastic modulus E_c	–	26,794.3 N/mm^2	–

Note: Tests on HCW subassemblies were performed approximately 100 days after concrete casting; consequentlyseveral concrete cubes were also tested within this timeframe.

3. Test results

The experimental programme consisted of a total of six tests (Table 2), with three performed on each of the two HCW configurations (*HCW_C-1* and *HCW_C-2*). After every test, only the shear link was replaced, while the wall, the external column and the threaded rods remained unchanged. This approach was intentional, as it reflects the expected behaviour in a real building structure following a seismic event - namely, that no damage should occur within the wall (except at its base, in case of walls fixed into foundations) or to the boundary steel columns.

This chapter presents the performance of the two HCW configurations under monotonic and cyclic loading, followed by a comparison of

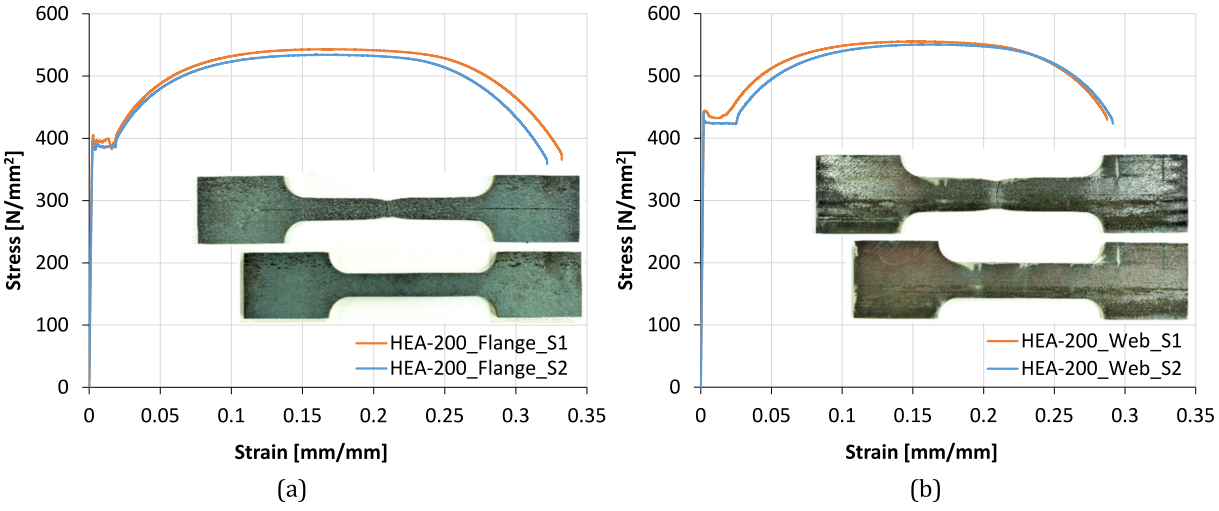

Fig. 8. Engineering stress-strain curves corresponding to the shear link: (a) flange; (b) web.

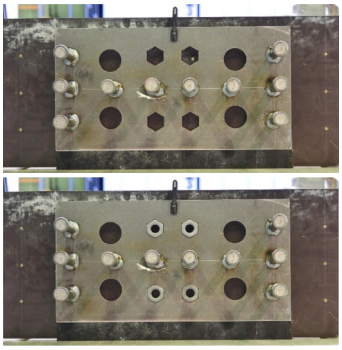

(a) Steel plates with shear studs to be embedded

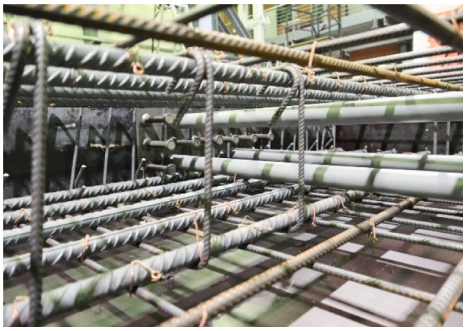

(b) RC wall reinforcement and plastic ducts for rods

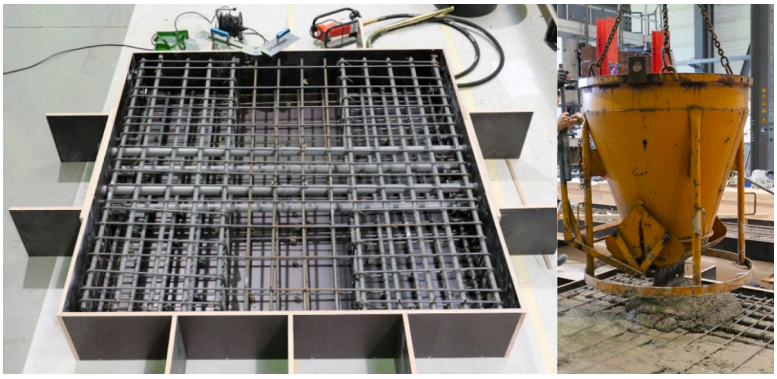

(c) Assembled formwork and reinforcement and concrete casting

(d) RC wall after concrete casting

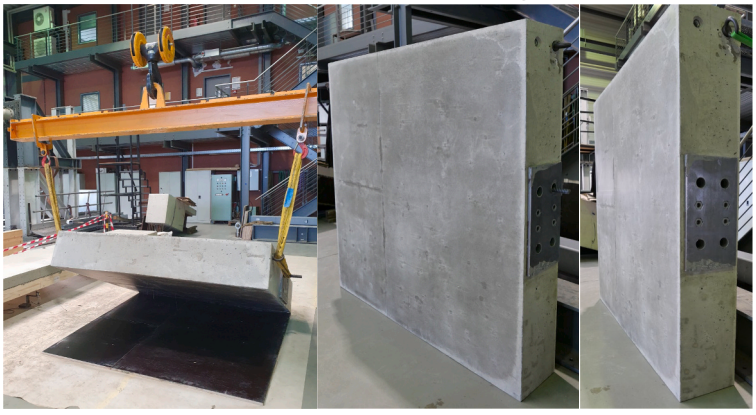

(e) Formwork removal

Fig. 9. Step-by-step fabrication and assembly procedure for the *HCW_C-1* specimens.

the results. Further details of the experimental tests on the HCW subsystems are documented in [46].

3.1. *Performance of HCW_Configuration-1*

The current section presents the response of the *HCW_C-1_M* specimen under monotonic loading, describing its initial state (Fig. 13), the post-tensioning force levels in the threaded rods before and during the test (Fig. 11), overall force–deformation response (Fig. 14), relative and local deformations of key connection components (Fig. 15a–c), and the specimen condition during and after testing (Fig. 16).

For the *HCW_C-1* specimens, the performance of the shear links was strongly influenced by the post-tensioning force applied to the threaded rods. While the connection between the shear link and the external column primarily transfers shear forces, the connection between the shear link and the RC wall was designed to transfer both shear forces and

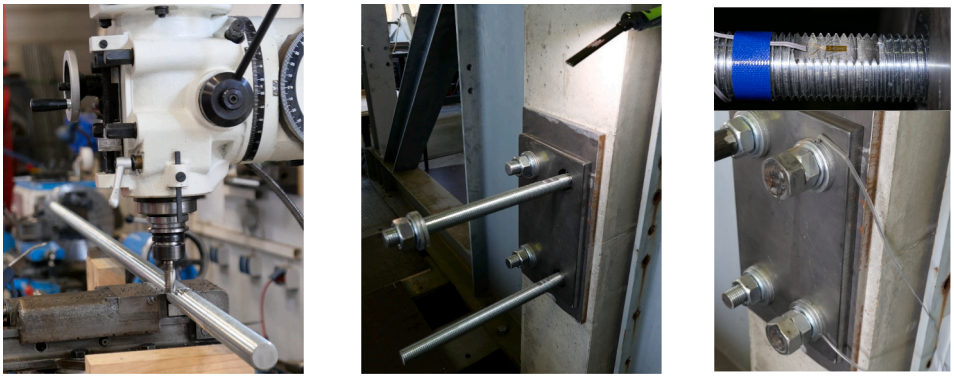

(f) Milling of the threaded rods, insertion into the RC wall, and instrumentation with strain gauges

(g) Assembly of test setup and post-tensioning of the threaded rods using a pneumatic torque wrench

Fig. 9. (*continued*).

bending moments.

As part of the pre-test finite element analysis (FEA), the required post-tensioning force for each M36 Gr. 8.8 threaded rod was determined using a design-assisted-by-FEM approach. A numerical model was developed to perform a sensitivity study in which the post-tensioning force in the threaded rods was the primary variable. Post-tensioning levels ranging from 0 kN up to the maximum allowable level for M36 Gr. 8.8 rods (i.e., 450 kN) were investigated.

The selected value of $F_{PT,Target} = 300$ kN was found to be optimal: higher pre-tensioning levels did not result in further improvement of the link performance, whereas lower levels reduced the effectiveness of the connection. Moreover, limiting the post-tensioning force to 300 kN prevented crushing of the concrete compression zone under the combined effects of post-tensioning in one row of threaded rods and compressive stresses induced by bending in the shear link.

The test instrumentation included force measurements in two threaded rods - specifically, one in the top and one in the bottom row. As shown in Fig. 11, this setup effectively captured the variation of strain and force over time. Although the positions of the threaded rods (TR) were kept in a steady position and the pressure in the HYTORC pneumatic torque tool was increased, the force levels in the rods could not be raised beyond a certain level. At the end of the post-tensioning phase, the recorded force levels were $F_{TR,Top} = 162.5$ kN and $F_{TR,Bottom} = 164.3$ kN, both significantly lower than the target force of 300 kN. Despite this discrepancy, it was decided to proceed with the testing phase, which consisted of monotonic loading—a complete cycle with ±40 mm deformation of the shear link (see Fig. 14 and Fig. 16).

The monotonic response of the *HCW_C-1_M* specimen is illustrated in Fig. 14, showing both the shear force–link displacement and the shear force–link rotation relationships. Due to tolerances in the connection between the link and the external column - including the presence of a filler plate - Fig. 14a shows that the deformations in the external column were slightly greater than those measured at the end of the shear link (i.e., at the end-plate; see Fig. 13c). It is worth noting that the end-plate holes were slightly oversized compared to the shop drawing specifications because they were flame-cut rather than drilled. This fabrication deviation likely contributed to the observed differences in deformation. As shown in Fig. 14a, the monotonic test enabled the evaluation of the shear link's stiffness, shear capacity, and nonlinear behaviour for displacements up to ±40 mm which corresponded to rotations of $\theta = \Delta/L = \pm 40/425 \times 1000 = \pm 94$ *mrad* (Fig. 14b).

The damage state of the *HCW_C-1_M* specimen during the test is shown in Fig. 16. As observed, the main deformations occurred within the shear link. Additionally, due to the presence of only two rows of threaded rods - located above and below the shear link - and the post-tensioning force being lower than the required $F_{PT,Target} = 300$ kN, deformations of the end-plate were also recorded during the test. These end-plate deformations (at the top and bottom flanges of the link) were measured throughout the experimental test, along with the relative deformations between the following components: (i) the external column and the shear link; (ii) the shear link and the embedded plate; (iii) the embedded plate and the concrete wall. The following values were recorded:

- The total relative deformation between external column and shear link was 6.5 mm (Fig. 15a);
- The total relative deformation between shear link and embedded plate was 1.1 mm (Fig. 15b);

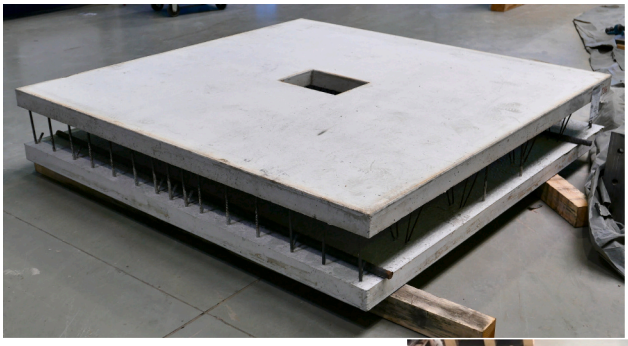

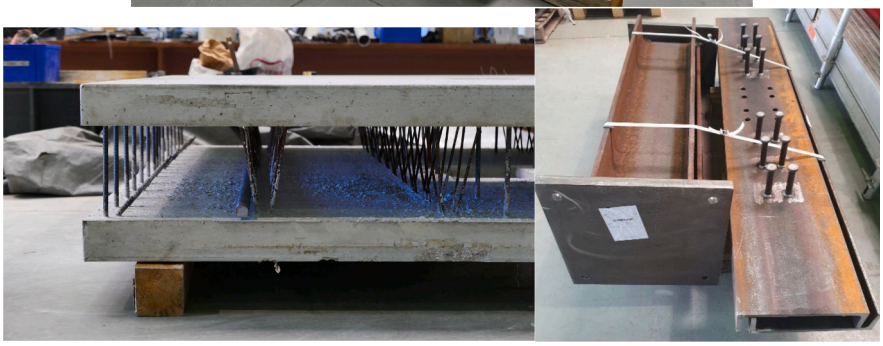

(a) Prefabrication and delivery of the elements (precast double-slab wall, encasing UPN profiles, external steel columns)

(b) Positioning of the RHS at wall center and of the threaded rods

(c) Positioning of the encasing UPN profiles, tightening of the threaded rods

Fig. 10. Step-by-step fabrication and assembly procedure of the *HCW_C-2* specimens.

(d) View from the inside of the wall (pre-casting) and on-site casting of the concrete infill

(e) Wall after concrete casting (f) Concrete hardening

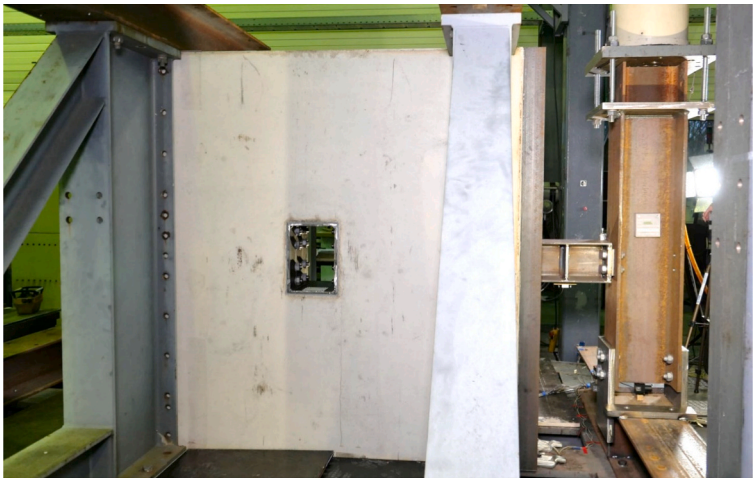

(g) Assembly of the test setup, including the *HCW_C-2* specimen

Fig. 10. (*continued*).

- The maximum gap between the embedded plate and the end-plate - attributed to local deformation of the end-plate under tensile forces - was 6.2 mm (Fig. 15c).

The current section also presents the response of the *HCW_C-1_C1* specimen under cyclic loading following the ECCS 1986 [44] protocol. The section describes the initial condition of the specimen (Fig. 17), the post-tensioning force levels in the threaded rods before and during the test (Fig. 12), the overall cyclic response -including comparison of force–deformation curves for the shear link and the external column (Fig. 18a) and the shear-force–link-rotation relationship (Fig. 18b), the relative and local deformations of key connection components (Fig. 19a–c), and the state of the specimen during and after testing (Fig. 20).

Similar to the *HCW_C-1_M* specimen, the test instrumentation for *HCW_C-1_C1* also included force measurements in two threaded rods (see Fig. 12). Following the post-tensioning phase, carried out using the HYTORC pneumatic torque system, the measured force in the top threaded rod was $F_{TR,Top} = 174.2$ kN, while the bottom threaded rod recorded $F_{TR,Bottom} = 172.4$ kN. Both values were lower than the target post-tensioning force ($F_{PT,Target} = 300$ kN). Despite this discrepancy, the decision was made to proceed with testing, which followed the ECCS-1986 [44] loading protocol (Fig. 18 and Fig. 20).

It should be emphasised that, since the post-tensioning forces were continuously monitored during the cyclic testing, the measurements indicated that the post-tensioning force remained stable throughout the loading protocol. For example, the force recorded in the bottom threaded rod at the end of the test (Fig. 12b) was essentially identical to the

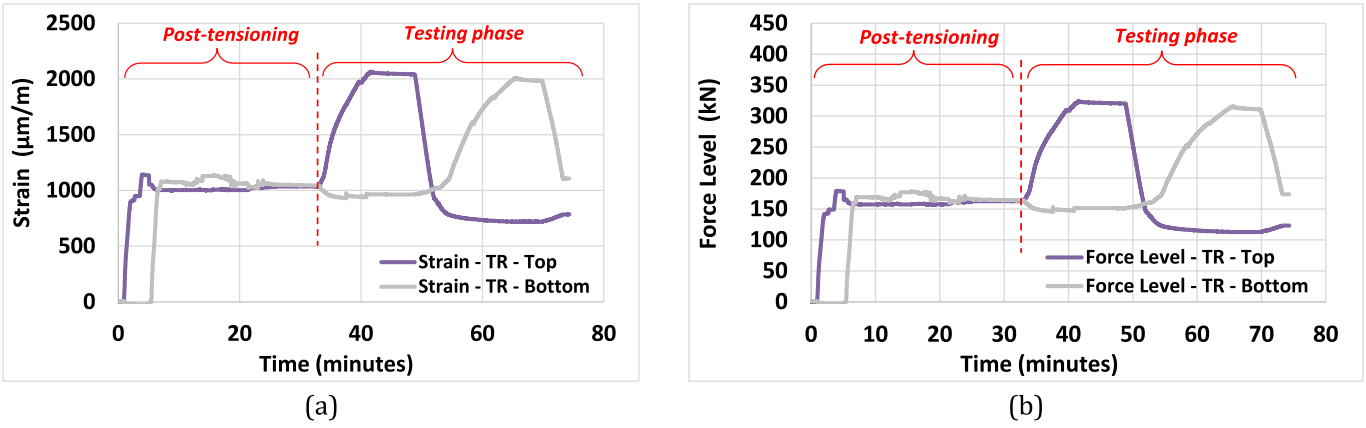

Fig. 11. Threaded rods of the *HCW_C-1_M* specimen before and during testing: (a) strain variation over time; (b) force variation over time.

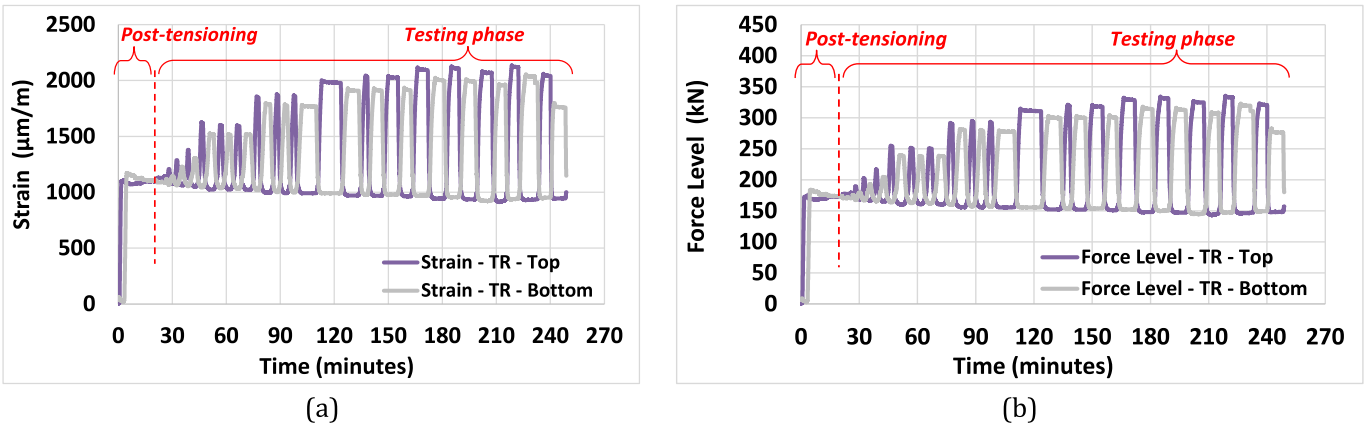

Fig. 12. Threaded rods of the *HCW_C-1_C1* specimen before and during testing: (a) strain variation over time; (b) force variation over time.

initial post-tensioning force applied prior to cyclic loading. No measurable prestress loss or relaxation was observed during the later stages of loading. Accordingly, neither the joint stiffness nor the overall hysteretic response of the subsystem was affected.

The cyclic response of the *HCW_C-1_C1* specimen is presented in Fig. 18, in terms of both shear force–link displacement and shear force–link rotation relationships. Owing to tolerances in the connection between the link and the external column, which incorporated a filler plate, the deformations recorded in the external column were slightly greater than those measured at the shear link end, as shown in Fig. 18a. With respect to the shear link response, the cyclic testing facilitated the characterization of stiffness, shear capacity, and nonlinear behaviour for displacements up to ±50 mm, or corresponding to rotations of up to $\theta = \Delta/L = \pm 50/425 \times 1000 = \pm 117$ *mrad* (see Fig. 18b).

The state of the *HCW_C-1_C1* specimen during testing is illustrated in Fig. 20. As observed, the primary deformations were limited to the shear link. In addition, due to the presence of only two rows of threaded rods (positioned above and below the shear link) and the applied post-tensioning force being lower than the target value ($F_{PT,Target} = 300$ kN), deformations of the end-plate were also recorded during the test. The end-plate deformations (corresponding to the top and bottom flanges of the link) were monitored, together with the relative deformations between: (i) the external column and the shear link; (ii) the shear link and the embedded plate; (iii) the embedded plate and the concrete wall. The following values were recorded:

- The total relative deformation between external column and shear link was 6.9 mm (Fig. 19a);
- The total relative deformation between shear link and embedded plate was 0.4 mm (Fig. 19b);
- The maximum gap between the embedded plate and the end-plate - attributed to local deformation of the end-plate under tensile forces - was 5.5 mm (Fig. 19c).

The performance of *HCW_C-1* specimens is detailed in Section 3.3.2, with emphasis on the global response, link deformation and cracking, end-plate and connection behaviour, performance of individual components.

3.2. Performance of HCW_Configuration-2

The current section presents the response of the *HCW_C-2_M* specimen under monotonic loading. The section describes the initial condition of the specimen prior to testing (Fig. 21), its overall response - including comparison of force–deformation curves for the shear link and the external column (Fig. 22a) and the shear-force–link-rotation relationship (Fig. 22b), the relative and local deformations of key connection components (Fig. 23a–c), and the damage state of the specimen during and after testing (Fig. 24).

The monotonic response of the *HCW_C-2_M* specimen is illustrated in Fig. 22, in terms of both shear force–displacement and shear force–rotation relationships. Due to tolerances in the link-to-side column connection, (which incorporated a filler plate), Fig. 22a shows that the deformations of the external column were slightly greater than those measured at the shear link end (i.e., end-plate). With respect to the shear link response, the monotonic test enabled the characterization of stiffness, shear capacity, and nonlinear behaviour for deformations up to

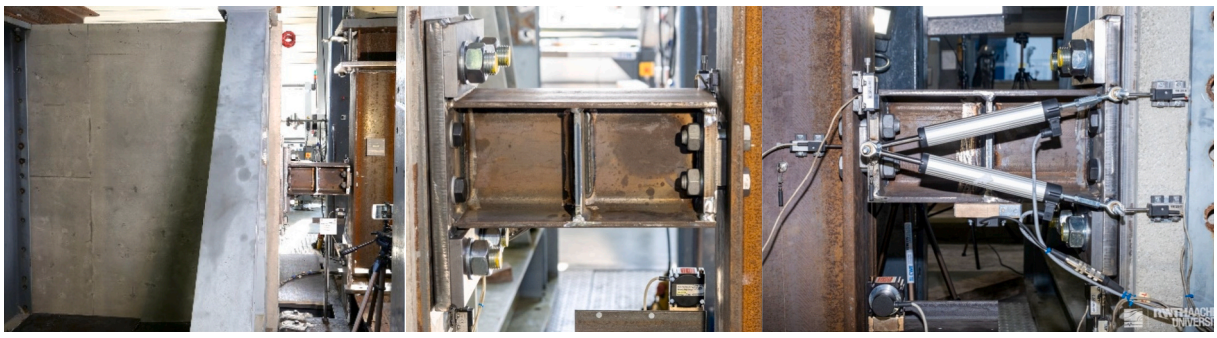

(a) (b) (c)

Fig. 13. State of the *HCW_C-1_M* specimen prior to testing: (a) overall view; (b) front view of the shear link; (c) back view of the shear link.

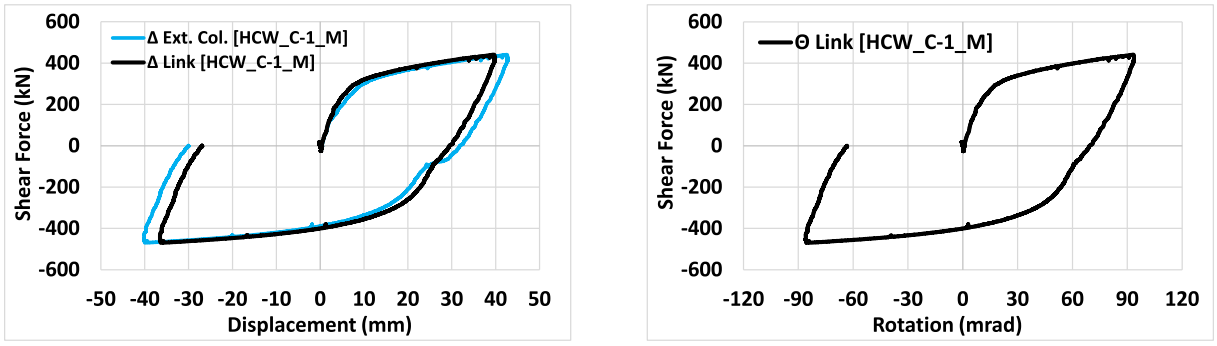

(a) (b)

Fig. 14. Response of the *HCW_C-1_M* specimen: (a) comparison of force-deformation curves for the shear link and external column; (b) shear force versus link rotation.

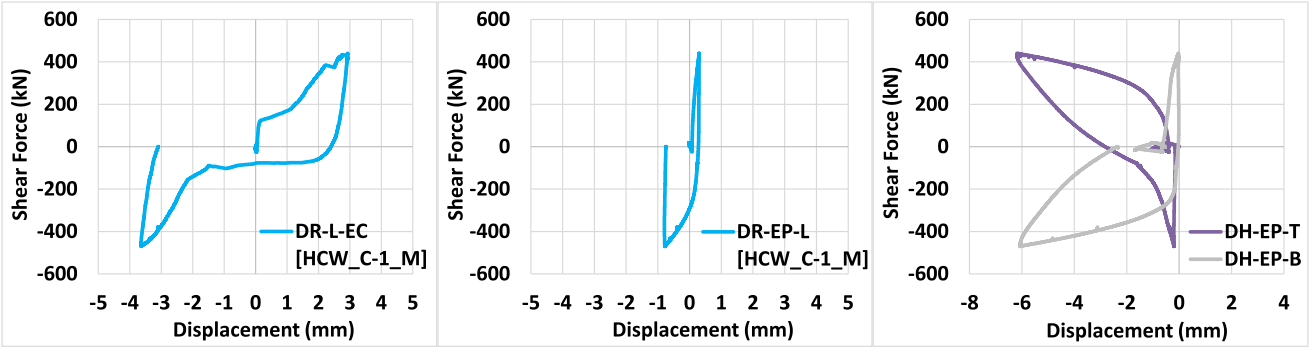

(a) (b) (c)

Fig. 15. Force versus relative/local deformation for the *HCW_C-1_M* specimen between: (a) the external column and shear link; (b) the shear link and embedded plate; (c) the end-plate and concrete wall.

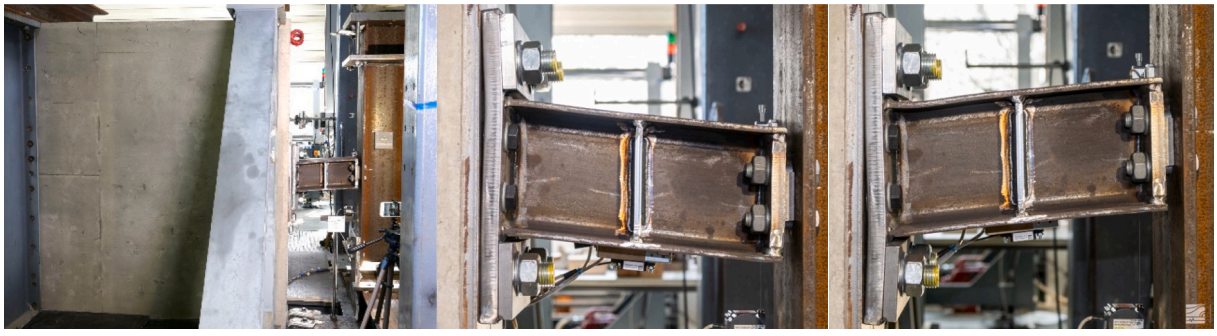

(a) (b) (c)

Fig. 16. State of the *HCW_C-1_M* specimen during testing: (a) overall view; (b) front view of the shear link at maximum downward deformation; (c) front view of the shear link at maximum upward deformation.

±40 mm, which corresponded to rotations up to ±94 mrad (Fig. 22b). The state of the *HCW_C-2_M* specimen during testing is illustrated in Fig. 24 which confirms that most deformations were limited to the shear link, as intended. The deformations of the end-plate (i.e., at the top and bottom flanges of the link) were recorded during testing, together with the relative deformations between: (i) the external column and the shear link; (ii) the shear link and the encasing UPN profile; (iii) the UPN profile and the concrete wall. The following results were obtained:

- The total relative deformation between external column and shear link was 5.8 mm (Fig. 23a);
- The total relative deformation between shear link and UPN profile was 0.3 mm (Fig. 23b);
- The maximum gap between the encasing UPN profile and the end-plate (local deformation of the end-plate under tension) was 2.0 mm (Fig. 23c).

The current section also presents the response of the *HCW_C-2_C1* specimen under cyclic loading. The section describes the initial condition of the specimen prior to testing (Fig. 25), its overall response - including comparison of force–deformation curves for the shear link and the external column (Fig. 26a) and the shear-force–link-rotation relationship (Fig. 26b), the relative and local deformations of key connection components (Fig. 27a–c), and the state of the specimen during and after testing (Fig. 28).

The *HCW_C-2_C1* specimen was tested following the ECCS-1986 [44] loading protocol, for which the yield displacement was determined from the monotonic response (d_y = 4.0 mm). The cyclic response of the *HCW_C-2_C1* specimen is illustrated in Fig. 26, in terms of both shear force–displacement (for the shear link and the external column) and shear force–rotation relationships. Due to tolerances in the link-to-side column connection, the deformations of the external column were slightly larger than those measured at the shear link end (i.e., end-plate), as shown in Fig. 26a. Regarding the shear link response, the cyclic test enabled the evaluation of stiffness, shear capacity and nonlinear hysteretic behaviour for deformations up to ±40 mm or rotations up to ±94 mrad (Fig. 26b). The state of *HCW_C-2_C1* specimen during testing is presented in Fig. 28, confirming that most deformations occurred within the shear link.

The deformations of the end-plate (i.e., at the top and bottom flanges of the link) were also recorded during the test together with the relative deformations measured between the: (i) external column and shear link; (ii) shear link and encasing UPN profile; (iii) encasing UPN profile and concrete wall. The following results were obtained:

- The total relative deformation between external column and shear link was 5.8 mm (Fig. 27a);
- The total relative deformation between shear link and UPN profile was 0.8 mm (Fig. 27b);
- The maximum gap between the encasing UPN profile and the end-plate (local deformation of the end-plate under tension forces) was 1.6 mm (Fig. 27c).

Further details with regard to the performance of *HCW_C-2* specimens are presented in Section 3.3.3, and focused on the following aspects: global response, link deformation and cracking, end-plate and general connection behaviour, as well as performance of individual components.

3.3. Comparison and discussion of results

The following section presents the comparison and discussion of the experimental results, with focus on both fabrication-related issues and structural performance of the specimens. To this end, the discussion is organized into four parts: (i) remarks on fabrication aspects (Section 3.3.1); (ii) performance assessment of the *HCW_C-1* specimens (Section 3.3.2); (iii) performance assessment of the *HCW_C-2* specimens (Section 3.3.3); and (iv) a comparative evaluation of the *HCW_C-1* and *HCW_C-2* specimens (Section 3.3.4). This structure allows for an appraisal of the key findings, while also facilitating the identification of similarities, differences and implications arising from the experimental programme.

3.3.1. Fabrication aspects

Regarding the fabrication of the *HCW_C-1* specimens (cast-in-situ wall with a post-tensioned wall-to-link connection), several advantages and limitations were identified. The system allows direct on-site fabrication and straightforward adaptation to the required geometry, including wall thickness, width, and other dimensional constraints. However, fabrication entails extensive formwork and on-site reinforcement placement, resulting in increased labour demand and larger volumes of in-situ concrete. Moreover, the post-tensioning of large-diameter and long (e.g., M36, grade 8.8, L = 2000 mm) threaded rods was very demanding, as the target pre-load was difficult to achieve in practice.

In the case of the *HCW_C-2* specimens (prefabricated wall with on-site concrete infill), no additional formwork is required, as the double-slab prefabricated wall and the encasing UPN profiles fully perform this function. On-site reinforcement assembly is eliminated, resulting in a faster construction with reduced manpower requirements compared to the cast-in-situ alternative. Overall fabrication time is shortened, and the presence of the encasing profiles may allow for a reduction in wall reinforcement. Furthermore, post-tensioning of medium-diameter threaded rods (M24 grade 10.9, or smaller) with shorter lengths (L = 1000 mm) is easier and can be carried out using manual torque wrenches. Conversely, prefabrication requires transportation and on-site storage of elements, unless a just-in-time delivery strategy is adopted.

In conclusion, the *HCW_C-1* configuration provides greater geometric flexibility but is labour-intensive and poses challenges for post-tensioning when large-diameter, long threaded rods are used. The *HCW_C-2* configuration offers clear advantages in construction speed, reduced on-site labour demand and ease of post-tensioning, at the expense of increased logistical requirements associated with the transportation and handling of the prefabricated elements.

3.3.2. Performance of HCW_C-1

For the *HCW_C-1* specimens, the primary objective was to ensure effective load transfer from the external steel column to the RC wall through the replaceable shear link. The shear link was designed to undergo significant plastic deformations and dissipate energy, while the remaining components (i.e., RC wall, threaded rods, external steel column) were expected to remain elastic. This configuration was intended to enable post-earthquake reparability by replacing only the damaged shear links.

The experimental investigations demonstrated an overall satisfactory structural performance of the *HCW_C-1* specimens, which is summarized further on in terms of global response, link behaviour and connection performance.

From a global response perspective, the shear force–deformation (F–Δ) relationships exhibited close agreement between monotonic and cyclic tests, together with a largely symmetric hysteretic response. Slightly larger displacements were recorded at the external column, attributable to fabrication tolerances at the bolted link-to-column connection. The maximum measured relative displacement reached 6.9 mm (±3.5 mm). Under the ECCS-1986 cyclic loading protocol [44], the shear link developed high initial stiffness, shear capacity and ductility, with deformations reaching ±50 mm (≈ ±117 mrad).

Regarding link deformation and cracking, the imposed loading induced pronounced shear deformations leading to the initiation of cracks at the welded stiffener-to-web connections. With increasing cyclic demand, these cracks propagated both horizontally and vertically

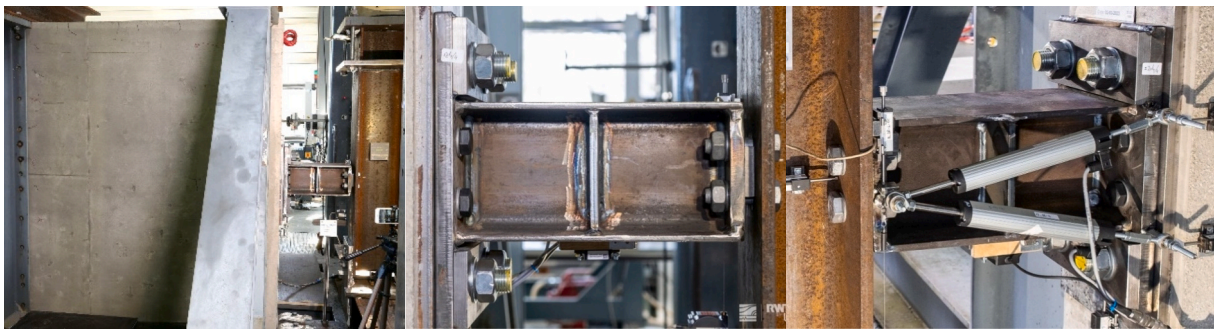

(a) (b) (c)

Fig. 17. State of the *HCW_C-1_C1* specimen prior to testing: (a) overall view; (b) front view of the shear link; (c) back view of the shear link.

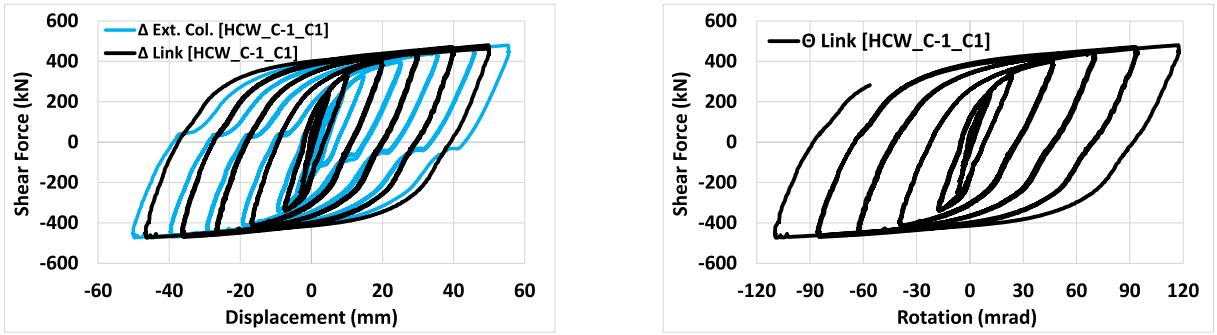

(a) (b)

Fig. 18. Response of the *HCW_C-1_C1* specimen: (a) comparison of force-deformation curves for the shear link and external column; (b) shear force versus link rotation.

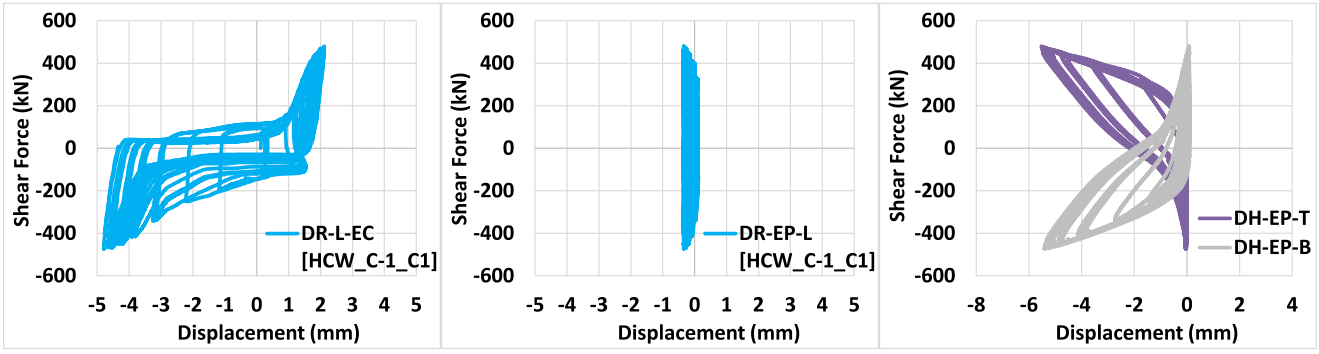

(a) (b) (c)

Fig. 19. Force versus relative/local deformation for the *HCW_C-1_C1* specimen between: (a) the external column and shear link; (b) the shear link and embedded plate; (c) the end-plate and concrete wall.

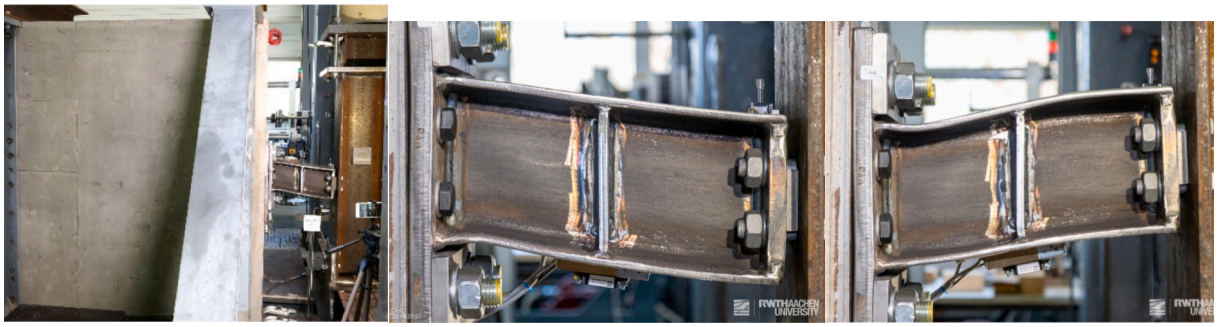

(a) (b) ±10·d_y | 2nd cycle (i.e., ±50mm)

Fig. 20. State of the *HCW_C-1_C1* specimen during testing: (a) overall view; (b) front view of the shear link at deformations of ±10•d_y (±50 mm).

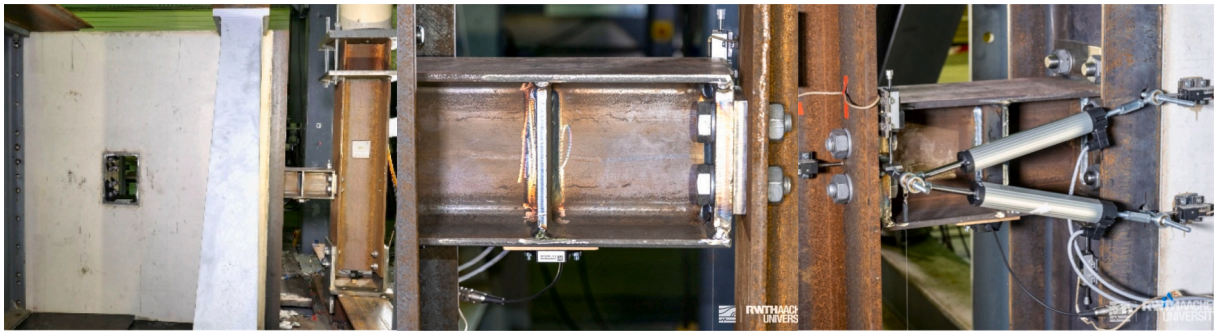

(a) (b) (c)

Fig. 21. State of the *HCW_C-2_M* specimen prior to testing: (a) overall view; (b) front view of the shear link; (c) back view of the shear link.

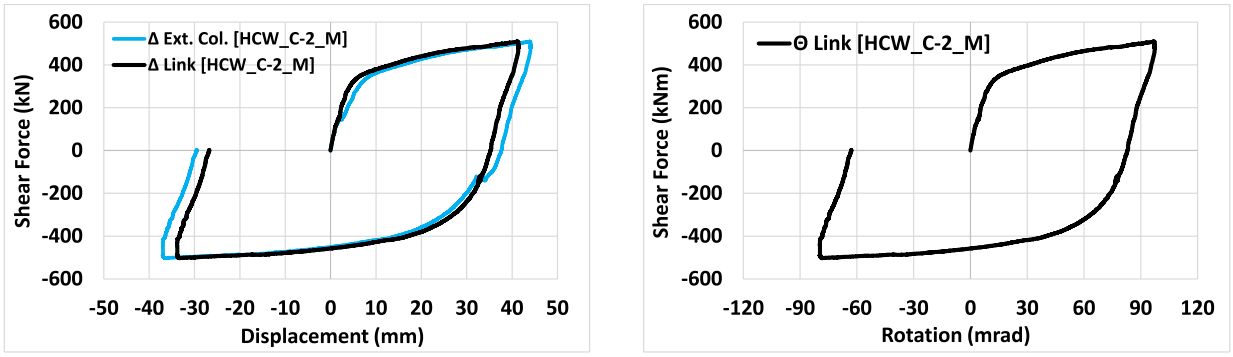

(a) (b)

Fig. 22. Response of the *HCW_C-2_M* specimen: (a) comparison of force-deformation curves for the shear link and external column; (b) shear force versus link rotation.

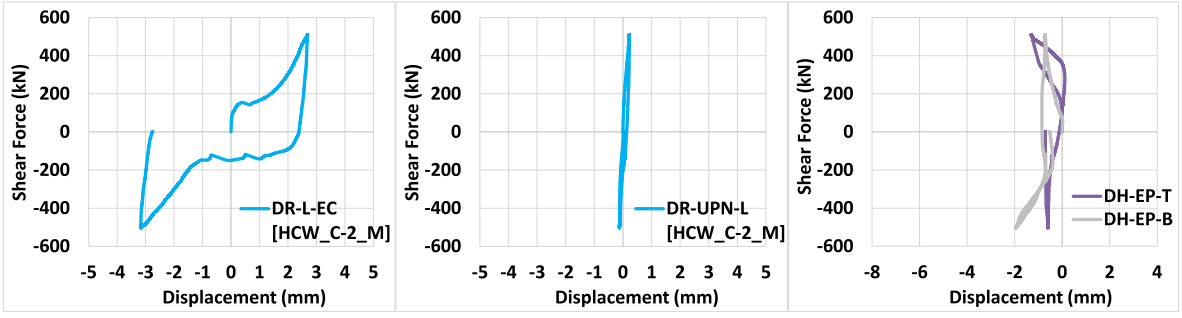

(a) (b) (c)

Fig. 23. Force versus relative/local deformation for the *HCW_C-2_M* specimen between: (a) the external column and shear link; (b) the shear link and encasing UPN profile; (c) the end-plate and UPN profile.

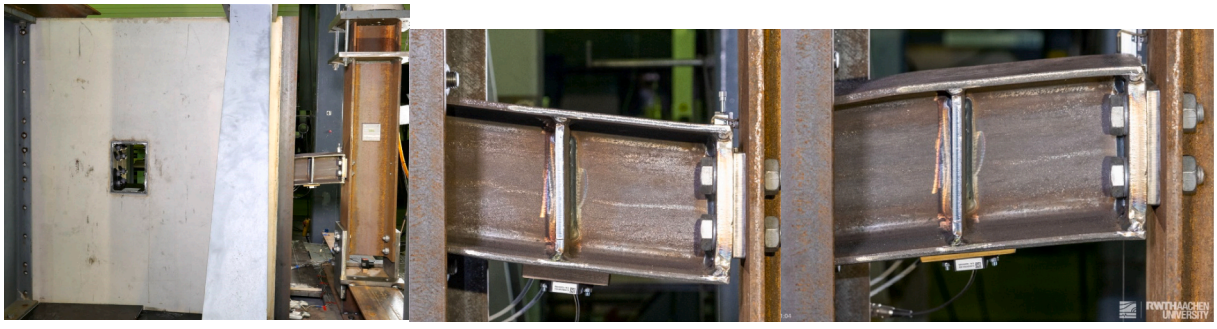

(a) (b) (c)

Fig. 24. State of the *HCW_C-2_M* specimen during testing: (a) overall view; (b) front view of the shear link at maximum downward deformation; (c) front view of the shear link at maximum upward deformation.

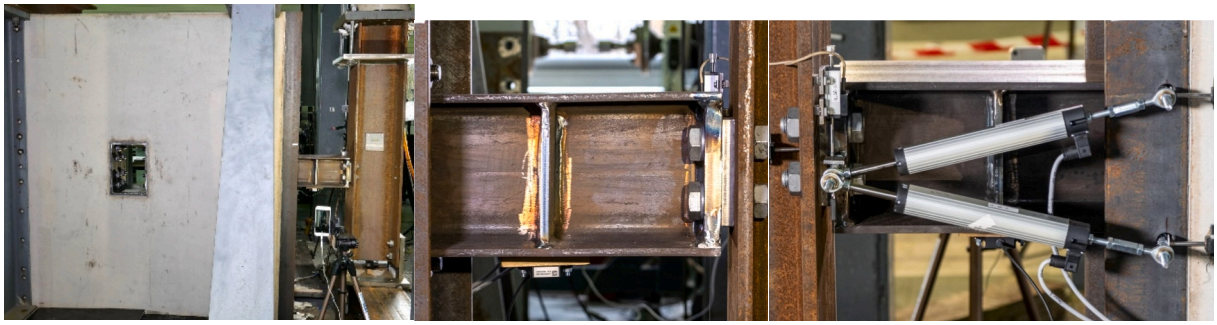

(a) (b) (c)

Fig. 25. State of the *HCW_C-2_C1* specimen prior to testing: (a) overall view; (b) front view of the shear link; (c) back view of the shear link.

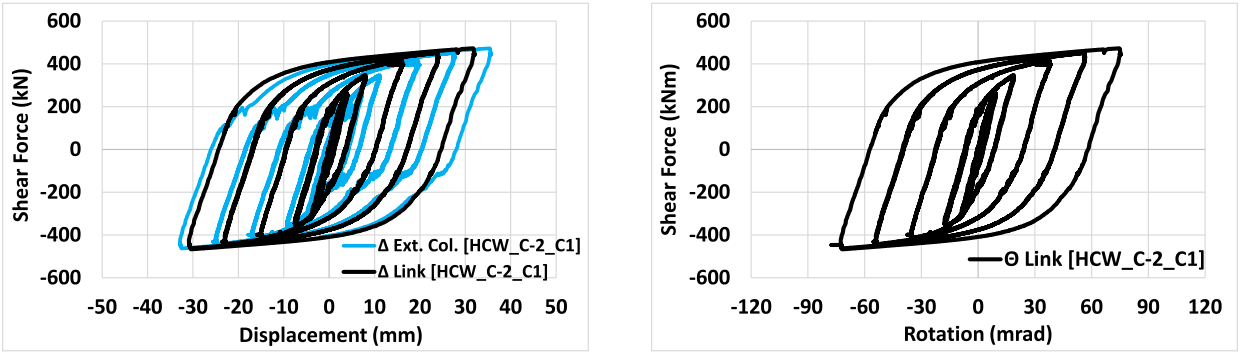

(a) (b)

Fig. 26. Response of the *HCW_C-2_C1* specimen: (a) comparison of force-deformation curves for the shear link and external column; (b) shear force versus link rotation.

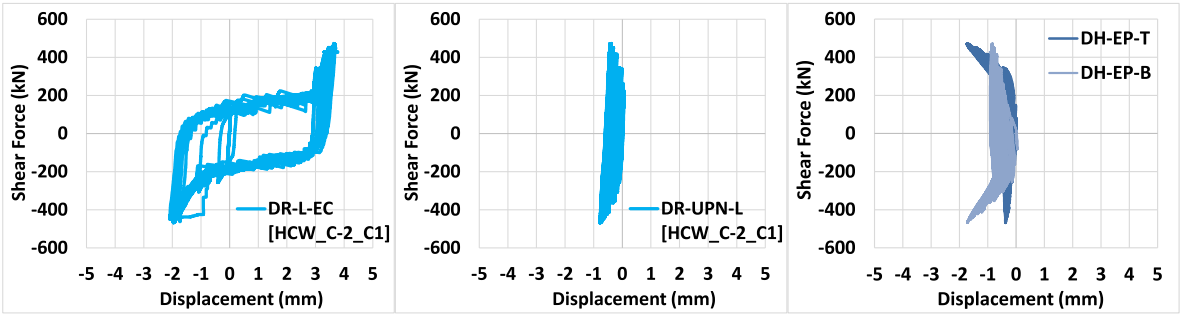

(a) (b) (c)

Fig. 27. Force versus relative/local deformation for the *HCW_C-2_C1* specimen between: (a) the external column and shear link; (b) the shear link and encasing UPN profile; (c) the end-plate and UPN profile.

(a) (b) ±10·d_y | 3rd cycle (i.e., ±40mm)

Fig. 28. State of the *HCW_C-2_C1* specimen during testing: (a) overall view; (b) front view of the shear link at deformations of ±10•d_y (±40 mm).

along the web, ultimately resulting in a progressive reduction of load-carrying capacity.

In addition to the link deformations, inelastic deformations ocurred in the end-plate connecting the link to the wall. This behaviour was attributed to insufficient post-tensioning of the threaded rods combined with the large distance between them (placed only above and below the shear link). As a consequence, the connection exhibited semi-rigid behaviour, with the end-plate contributing to both deformation and energy dissipation. Local deformations were quantified by a maximum relative displacement of 0.40 mm between the shear link and the embedded plate, 0.21 mm between the embedded plate and the RC wall, and a maximum opening of 6.2 mm between the end-plate and the embedded plate (due to tension deformation of the end-plate).

The assessment of individual components further confirmed the intended failure mechanism. Post-tensioning of the large-diameter M36 grade 8.8 threaded rods proved difficult, despite using a HYTORC pneumatic torque system. The rod size resulted from the initial design, which envisioned two rows of post-tensioned tendons stressed using hydraulic jacks. However, geometric constraints prevented jack placement between the flanges, restricting stressing operations to locations above or below the shear link and compromising the preload levels.

The RC wall remained elastic throughout the three tests, with no evidence of cracking or crushing, thereby confirming the intended damage localization within the shear link. The embedded plate connection with welded shear studs ensured effective composite action with the RC wall, as evidenced by relative displacements consistently below 0.21 mm. The link-to-column connection efficiently transferred shear forces without inducing significant bending moments, behaving as a simple shear connection. Nevertheless, fabrication tolerances associated with oversized end-plate holes resulted in a total relative displacement of 6.9 mm, which could be mitigated through tighter tolerances.

Finally, the shear link successfully fulfilled its role as the primary energy-dissipating component, developing large plastic deformations. Only limited plastic deformations occurred within the end-plate. All other components remained elastic, and the external column did not exhibit global deformations, despite minor plastic ovalization of the bolt holes ($\approx$ 0.5 mm) after removal of the shear link.

Consequently, the *HCW_C-1* specimens successfully validated the design objective by concentrating inelastic demand within the shear link, thereby protecting the surrounding structural components. The system exhibited high ductility and significant energy dissipation capacity. However, some practical challenges were identified (post-tensioning of large-diameter threaded rods, fabrication tolerances), highlighting the need for targeted refinements in detailing and construction practices to further improve structural performance and reliability.

3.3.3. Performance of HCW_C-2

Regarding the *HCW_C-2* specimens, the objective was identical to that of *HCW_C-1*.

Experimental investigations confirmed the satisfactory structural performance of the *HCW_C-2* configuration, which is discussed further on in terms of global response, link behaviour, local deformations, and component-level performance.

From a global response standpoint, the shear force–deformation (F–Δ) curves showed close agreement between monotonic and cyclic tests, together with a largely symmetric response. Slightly larger-than-expected displacements were recorded at the external column, yet these were attributable to fabrication tolerances at the bolted link-to-column connection. The maximum relative displacement was 5.8 mm (±2.9 mm). Under both the ECCS-1986 [44] and EN 15129 [45] cyclic loading protocols, the shear link developed high initial stiffness, shear capacity and ductility. Using the ECCS-1986 protocol, maximum deformations of ±40 mm ($\approx$ ±94 mrad) were attained. Under the EN 15129 protocol, the shear link sustained the prescribed cyclic history without strength or stiffness degradation, including 5 cycles at $\pm 25\% \cdot d_{bd}$, 5 cycles at $\pm 50\% \cdot d_{bd}$, and 10 cycles at $\pm 100\% \cdot d_{bd}$, where the design deformation $d_{bd} = 24$ mm was derived using the *HCW_C-2* specimen geometry and the interstory drift limit of 15 mrad for braced frames at Significant Damage limit state.

Regarding the link deformation and cracking (Fig. 29), the imposed loading induced pronounced shear deformations leading to the initiation of cracks at the welded connection between the stiffener and link web, consistent with the observations for *HCW_C-1*. With increasing demand, these cracks propagated both horizontally and vertically along the web, ultimately resulting in a reduction of the shear capacity.

Local deformation demands remained limited. The maximum relative displacement between the shear link and the encasing UPN profile was 0.8 mm, while the relative displacement between the UPN profile and the wall remained below 0.1 mm. In addition, the maximum opening between the end-plate and the UPN profile, associated with deformations of the end-plate under tension, did not exceed 1.6 mm.

The performance of individual components further corroborated the intended design strategy. The M24 grade 10.9 threaded rods were relatively easy to post-tension using a manual torque wrench, confirming the constructability advantages of the adopted detailing. The steel–concrete composite wall remained undamaged throughout the three tests, with no evidence of cracking or crushing, thereby confirming that damage was confined to the shear link. The UPN profile–to–wall connection (realised using welded shear studs; Fig. 10a,d), ensured effective anchorage to the concrete core, with relative deformations below 0.1 mm.

The link-to-column connection successfully transferred shear forces while acting as a simple shear connectionwith negligible bending moments. Nevertheless, oversized bolt holes in the end-plate resulted in relative displacements of up to 5.8 mm, suggesting that tighter fabrication tolerances could further improve performance. As intended, the shear link acted as the main energy-dissipating fuse, developing large plastic deformations, while all other components remained elastic. The side column did not exhibit global deformations, in spite of minor plastic ovalization of the bolt holes ($\approx$ 0.5 mm).

In conclusion, the *HCW_C-2* specimens exhibited adequate structural performance, fulfilling the design objective of concentrating inelastic demand within the shear link while preserving elastic behaviour in the surrounding components. Relative to *HCW_C-1*, the *HCW_C-2* configuration facilitated easier post-tensioning of the threaded rods and resulted in smaller end-plate deformations. However, fabrication tolerances in the link-to-column connection continued to influence the measured relative displacements. Overall, the results underscore the efficiency of the *HCW_C-2* configuration in achieving high ductility and reparability, while minor refinements in detailing are needed to further enhance structural performance.

3.3.4. Comparison between HCW_C-1 and HCW_C-2

A direct comparison between the *HCW_C-1* and *HCW_C-2* specimens was performed by examining the shear force–deformation (F–Δ) responses under monotonic and cyclic loading (Fig. 30a–b). The failure modes observed in the monotonic tests (*HCW_C-1_M* and *HCW_C-2_M*) are compared in Fig. 30c.

Referring to the monotonic responses (Fig. 30a, Fig. 30c), the two configurations shared identical shear link geometries (cross-section, length, and stiffener layout) and identical link-to-column connections, while differing only in the link-to-wall connection. In this context, the post-tensioning arrangement was found to exert a decisive influence on the structural response. In *HCW_C-1*, two rows of post-tensioned M36 grade 8.8 threaded rods led to a relatively low effective pre-load, which resultedin a slight reduction in initial stiffness and load-carrying capacity. This response was associated with pronounced end-plate deformations, manifested by measured gaps of approximately 6.0 mm (Fig. 30c). By contrast, *HCW_C-2* employed four rows of shorter, smaller-diameter threaded rods (M24 grade 10.9), which provided improved

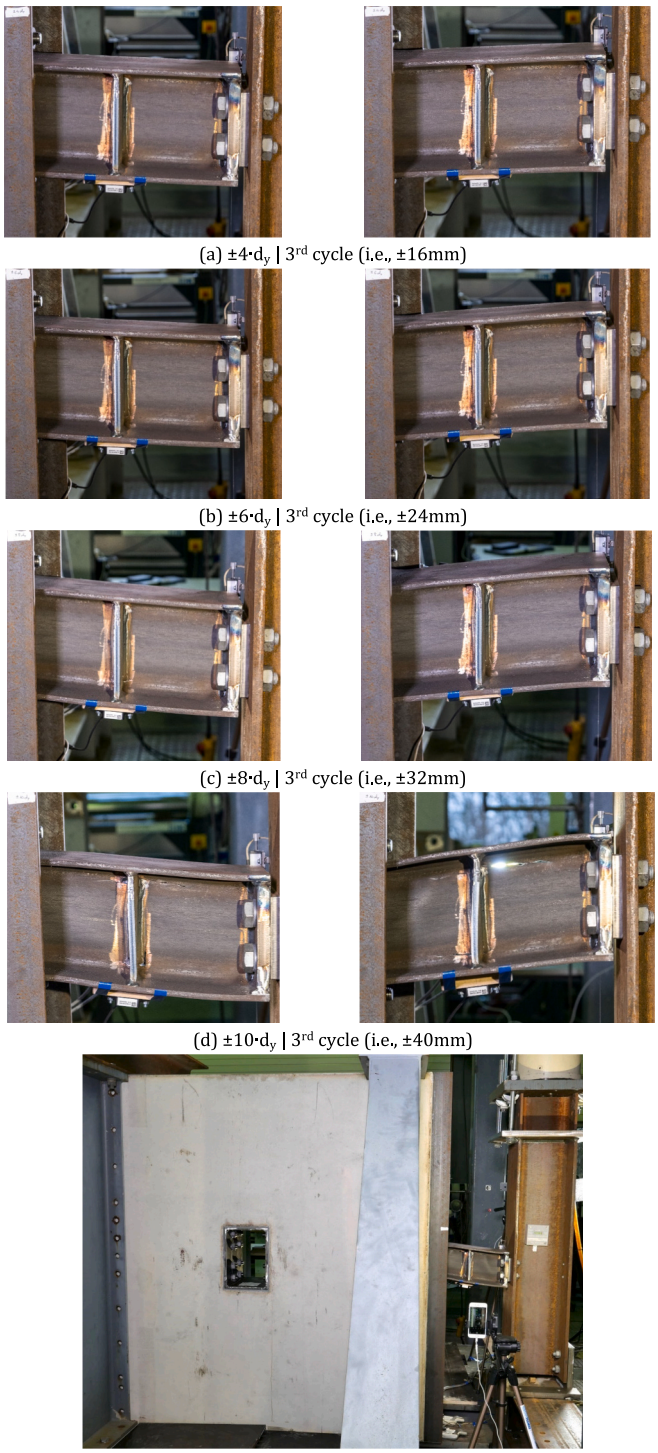

(a) ±4·d_y | 3rd cycle (i.e., ±16mm)

(b) ±6·d_y | 3rd cycle (i.e., ±24mm)

(c) ±8·d_y | 3rd cycle (i.e., ±32mm)

(d) ±10·d_y | 3rd cycle (i.e., ±40mm)

(e) overall view of the specimen

Fig. 29. Evolution of damage in specimen *HCW_C-2_C1* during testing using the ECCS 1986 [44] loading protocol: front views of the shear link at deformations of ±4·d_y, ±6·d_y, ±8·d_y, and ± 10·d_y; (e) overall view of the specimen.

end-plate restraint and promoted the concentration of inelastic deformations within the shear link. Thus, *HCW_C-2* exhibited higher stiffness and resistance.

Under cyclic loading (Fig. 30b), both configurations displayed stable hysteretic behaviour with comparable symmetry and energy dissipation capacity, despite some differences in deformation capacity. *HCW_C-2* sustained deformations up to ±40 mm (≈ ±94 mrad), whereas *HCW_C-1* reached a larger deformation capacity of ±50 mm (≈ ±117 mrad). The resulted difference reflects more flexibilityof the *HCW_C-1* link-to-wall connection, which allowed for additional deformation at the expense of stiffness.

The observed failure modes (Fig. 30c) further highlight the influence of the connection detailing. In *HCW_C-1*, the failure mechanism involved significant end-plate deformations, arising from the limited post-tensioning force. In contrast, the *HCW_C-2* specimens exhibited a more favourable failure mode, with inelastic deformations predominantly concentrated within the shear link, fully consistent with the intended design philosophy.

The comparative results underscore the critical role of the link-to-wall connection in governing global stiffness, strength and failure mechanism. The *HCW_C-1* configuration, while achieving slightly greater deformation capacity, exhibited lower stiffness and resistance due to end-plate flexibility. Conversely, the *HCW_C-2* configuration demonstrated superior stiffness and load-carrying capacity, with inelastic deformations more effectively localized within the shear link - an outcome attributable to the optimized arrangement of the threaded rods in terms of number, diameter and length.

3.3.5. *Positioning of HCWs relative to conventional seismic systems*

HCWs incorporating replaceable steel shear links represent a structural system that combines RC walls with ductile steel elements. In order to clarify the motivation for adopting this system, it would be useful to position HCWs relative to more conventional seismic-resistant systems such as steel eccentrically braced frames (EBFs) and concentrically braced frames with buckling-restrained braces (CBF with BRBs).

However, a rigorous quantitative comparison between different structural systems would require designing alternative solutions for the same building configuration (identical seismic hazard, geometry, height and performance objectives). Such an investigation falls beyond the scope of the present experimental study. Nevertheless, the main conceptual distinctions between the proposed HCW system and conventional steel-based solutions are summarized below.

Global stiffness and drift control. Compared with steel-only systems such as EBFs or CBFs with BRBs, the inclusion of RC walls significantly increases the global lateral stiffness of the structural system. This can be particularly advantageous in mid- to high-rise buildings (e.g., 10–20 storeys), where interstorey drift limitations often govern the design. Achieving comparable stiffness using a bare steel system would require larger structural members and, thus, increased steel consumption.

Energy dissipation and reparability. Similar to EBFs, HCWs limit seismic energy dissipation to designated steel components, namely replaceable shear links. However, unlike conventional EBF configurations, the RC wall provides additional stiffness and strength while maintaining the replaceability of the primary dissipative element. In contrast, although systems with BRBs offer stable hysteretic behaviour, replacement of damaged braces may require more extensive intervention within the structural frame. Overall, the HCW system is not intended to replace conventional EBF or CBF systems with BRBs. Instead, it provides an alternative solution for buildings where enhanced stiffness, improved drift control and controlled energy dissipation through replaceable steel elements are desirable.

Structural robustness and redundancy. The hybrid configuration combines the robustness and inherent damping of RC walls with the ductile and well-defined plastic yielding of steel shear links. This combination allows the global stiffness and strength of the system to be provided primarily by the walls, while seismic energy dissipation is concentrated in the steel links. This separation between the primary lateral-load-resisting elements and the designated dissipative components can improve structural robustness and facilitate damage control.

Constructability considerations. The inclusion of RC walls introduces additional construction steps compared with a bare steel frame. However, hybrid construction is widely used in many regions, particularly in buildings where RC cores or walls are already required for

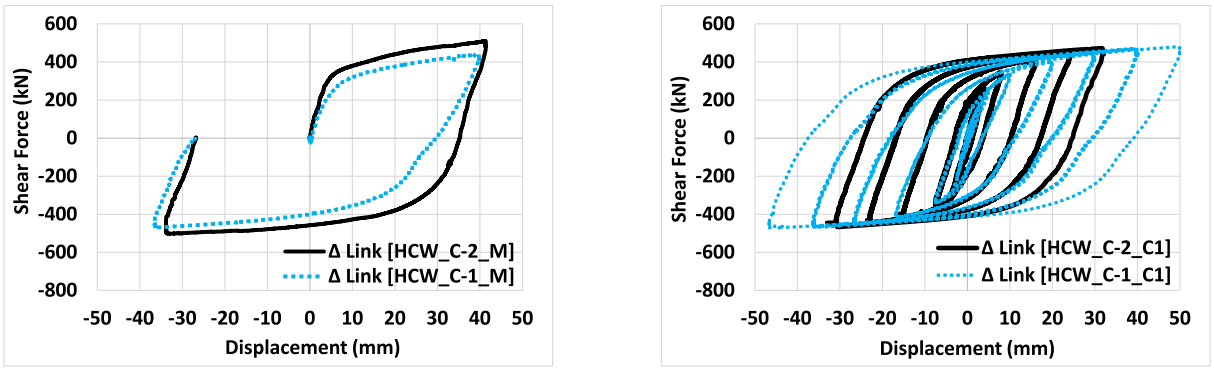

(a) comparison of the monotonic response

(b) comparison of the cyclic response

(c) comparison of failure modes for *HCW_C-1_M* and *HCW_C-2_M* specimens

Fig. 30. Comparison of (a) monotonic and (b) cyclic responses of specimens *HCW_C-1* and *HCW_C-2*; (c) comparison of failure modes for *HCW_C-1_M* and *HCW_C-2_M* specimens.

gravity loads or serviceability considerations. The proposed HCW system aims to maintain simplicity at the interface between steel and concrete through bolted connections and accessible replaceable links, thereby facilitating post-earthquake inspection and repair.

Wall-base damage and implications for reparability. There are at least two possible scenarios.

Scenario 1: HCWs with pinned walls.

In the context of post-earthquake reparability, the global structural response - including residual displacements - has been investigated by the authors within the broader research programme. Preliminary results are reported in [47], with an extended study currently under development. In particular, a case-study building with pinned HCWs combined with moment-resisting frames (MRFs) was analysed through nonlinear static and dynamic analyses. For the investigated configuration, which is similar to the existing building structure reported in [48], combined with re-centring MRF as validated in [49] - the predicted residual drifts and residual link deformations are not expected to hinder practical link replacement following a design-level seismic event.

Scenario 2: HCWs with fixed walls.

In systems combining RC walls with steel dissipative elements, the relatively high stiffness of the walls may result in significant force demands at the wall base, potentially leading to cracking or yielding prior to the activation of the steel shear links. This raises the question of whether damage at the wall base could compromise the intended repairability of the system. While this concern may be relevant for certain fixed-base configurations, it should be emphasised that the proposed system is intended to be applied within a performance-based design framework, in which significant damage to the RC walls is expected only at higher performance levels (Near Collapse). Experimental evidence supporting this behaviour has been obtained from cyclic testing of a half-scale four-storey building specimen [50], the detailed results of which will be presented in a publication currently in preparation.

Implications of multiple plastic mechanisms for design. In hybrid systems combining RC walls and steel shear links, the possibility that plastic hinges may develop both at the wall base and within the shear links raises questions regarding the complexity of the design procedure and the appropriate global ductility factor. Two main scenarios can be considered. In configurations with pinned wall bases, seismic energy is primarily dissipated in the shear links, while the global structural behaviour can be considered analogous to that of an EBF. In this case, the design procedure remains relatively straightforward and the global ductility factor may be taken as that typically associated with EBFs.

For configurations with fixed wall bases, plastic hinges may develop both at the wall base and in the shear links, resulting in a dual energy-dissipation mechanism. In such cases, the assignment of a global ductility factor requires careful evaluation, as interaction between the two nonlinear mechanisms must be considered and compatibility between wall plastic rotations and link deformations must be verified. Parametric investigations carried out within the HYCAD research project indicate that, depending on the targeted coupling ratio and the building height, behaviour factors in the range of approximately $q = 3.0–6.0$ may be achieved. For a conservative design approach, a value of $q = 3.0$ may be adopted, while higher values may be justified based on more detailed system-level assessments and design guidance developed within the research programme.

4. Conclusions

This paper presents the results of an experimental investigation of hybrid coupled wall systems with replaceable shear links, by comparing

two alternative configurations: *HCW_C-1* (cast-in-situ wall with post-tensioned connection) and *HCW_C-2* (prefabricated wall with on-site concrete infill). The study analysed both fabrication aspects and structural performance under monotonic and cyclic loading, focusing on the connection of the shear links to the RC/composite wall, the test program and specimen layouts, and the response of individual components.

Both configurations were designed to transfer loads from the external column to the wall through the replaceable shear link, with the link undergoing large plastic deformations while the remaining components - RC/composite wall, threaded rods and external steel column - remained elastic. This approach was followed to enable post-seismic event reparability by replacing the damaged links. The most interesting observations and main conclusions are summarized as follows:

Fabrication-related aspects:

- *HCW_C-1* provides geometric flexibility and full on-site constructability, but requires extensive formwork, reinforcement assembly and large in-situ concrete volumes. Achieving the required pre-load in large-diameter, long threaded rods proved challenging, rendering the process labour-intensive.
- *HCW_C-2* offers faster construction, reduced labour requirements and easier post-tensioning of smaller, shorter rods using simpler tools, though its main limitation is the logistical demand for transporting and storing prefabricated elements.

Structural performance:

- *HCW_C-1* validated the design strategy, as inelastic deformations were limited to the shear link while other components remained elastic. The system exhibited high ductility and energy dissipation capacity, but limited post-tensioning of the large rods and their restricted placement led to notable end-plate deformations, slightly reducing the stiffness and the resistance.
- *HCW_C-2* demonstrated stable monotonic and cyclic response, high ductility and symmetric force–deformation behaviour. The optimized arrangement of smaller, shorter rods (four rows of M24 grade 10.9 rods) enabled reliable post-tensioning, reduced end-plate deformations, and ensured inelastic demand remained confined to the shear link. The composite wall and external column remained elastic, underscoring the system's reparability potential. Minor relative displacements at the link-to-column connection were linked to bolt hole tolerances. The shear links performed consistently under both ECCS-1986 [44] and EN 15129 [45] cyclic protocols, reaching deformations of ±40 mm (rotation of ±94 mrad) without loss of stiffness, strength or ductility. Cracks initiated at the web-to-stiffener weld propagated gradually but did not compromise overall performance.

Comparison of configurations:

While both configurations validated the concept of repairable hybrid coupled walls, some differences between them should be noted. *HCW_C-1* achieved slightly higher deformation capacity (±50 mm) but at the expense of reduced stiffness and strength, reflecting the flexibility of its link-to-wall connection. *HCW_C-2*, in contrast, exhibited superior stiffness and load-carrying capacity, with inelastic deformations effectively localized within the shear link, and negligible end-plate deformations, attributable to the optimized rod arrangement in terms of diameter, length, and number.

In conclusion, the experimental results confirm the feasibility of the proposed repairable HCW systems. While both HCW configurations successfully concentrated inelastic demand within replaceable shear links, the prefabricated *HCW_C-2* configuration provides superior constructability, stiffness and structural performance, fully consistent with the intended design philosophy.

CRediT authorship contribution statement

Cristian Vulcu: Writing – original draft, Visualization, Methodology, Investigation, Formal analysis, Data curation. **Rajarshi Das:** Writing – review & editing, Project administration, Funding acquisition. **Rafaela Don:** Writing – review & editing, Writing – original draft, Visualization, Investigation. **Benno Hoffmeister:** Writing – review & editing, Supervision, Resources, Project administration, Funding acquisition. **Hervé Degée:** Writing – review & editing, Supervision, Project administration, Funding acquisition, Conceptualization.

Declaration of competing interest

The authors declare that they have no known competing financial interests or personal relationships that could have appeared to influence the work reported in this paper.

Acknowledgements

Funded by the European Union. The research activities were performed in the framework of the HYCAD research project, which has received funding from the Research Fund for Coal and Steel (RFCS) under GA No. 899381. This financial support is gratefully acknowledged. Views and opinions expressed are however those of the authors only and do not necessarily reflect those of the European Union or the Research Fund for Coal and Steel. Neither the European Union nor the Research Fund for Coal and Steel can be held responsible for them.

Data availability

The experimental database, upon which the current work is based, can be made available from the corresponding author upon reasonable request.

References

[1] H. Bernhardt, M. Kuhnhenne, R.M. Lawson, M. Veljkovic, Sustainable Steel Buildings: A Practical Guide for Structures and Envelopes, John Wiley & Sons, 2016. ISBN 9781118740798.
[2] T. Paulay, Coupling beams of reinforced concrete shear walls, J. Struct. Div. 97 (3) (1971) 843–862, https://doi.org/10.1061/JSDEAG.0002848.
[3] T. Paulay, A. Santhakumar, Ductile behavior of coupled shear walls, J. Struct. Div. 102 (1) (1976) 93–108, https://doi.org/10.1061/JSDEAG.0004279.
[4] S.A. Mahin, V.V. Bertero, Nonlinear seismic response of a coupled wall system, J. Struct. Div. 102 (9) (1976) 1759–1781, https://doi.org/10.1061/JSDEAG.0004428.
[5] W.-S. Park, H.-D. Yun, Seismic behaviour of steel coupling beams linking reinforced concrete shear walls, Eng. Struct. 27 (2005) (2005) 1024–1039, https://doi.org/10.1016/j.engstruct.2005.02.013.
[6] T. Holden, J. Restrepo, J.B. Mander, Seismic performance of precast reinforced and prestressed concrete walls, J. Struct. Eng. 129 (3) (2003) 286–296, https://doi.org/10.1061/(ASCE)0733-9445(2003)129:3(286).
[7] K. Harries, B.M. Shahrooz, Hybrid coupled wall systems, ACI Concr. Int. 27 (5) (2005) 45–51.
[8] Q. Shen, Y.C. Kurama, Nonlinear behavior of posttensioned hybrid coupled wall subassemblages, J. Struct. Eng. 128 (10) (2002) 1290–1300, https://doi.org/10.1061/(ASCE)0733-9445(2002)128:10(1290).
[9] P.J. Fortney, B.M. Shahrooz, G.A. Rassati, Large-scale testing of a replaceable "fuse" steel coupling beam, J. Struct. Eng. 133 (12) (2007) 1801–1807, https://doi.org/10.1061/(ASCE)0733-9445(2007)133:12(1801).
[10] H. Hu, J. Liu, G. Cheng, J. Li, Y.F. Chen, Seismic behavior of hybrid coupled wall system with replaceable endplate-steel coupling beam, J. Constr. Steel Res. 187 (2021) 106997, https://doi.org/10.1016/j.jcsr.2021.106997.
[11] D. Xu, B. Xiang, X. Chong, K. Xu, J.-B. Yan, T. Wang, Seismic performances of the joint between replaceable-coupling beams and composite shear wall, J. Constr. Steel Res. 197 (2022) 107462, https://doi.org/10.1016/j.jcsr.2022.107462.
[12] S. El-Tawil, K. Harries, P.J. Fortney, B.M. Shahrooz, Y. Kurama, Seismic design of hybrid coupled wall systems: state of the art, J. Struct. Eng. 136 (7) (2010) 755–769, https://doi.org/10.1061/(ASCE)ST.1943-541X.0000186.
[13] D. Dan, A. Fabian, V. Stoian, Theoretical and experimental study on composite steel–concrete shear walls with vertical steel encased profiles, J. Constr. Steel Res. 67 (2011) (2011) 800–913, https://doi.org/10.1016/j.jcsr.2010.12.013.
[14] D. Dan, A. Fabian, V. Stoian, Nonlinear behavior of composite shear walls with vertical steel encased profiles, Eng. Struct. 33 (2011) 2794–2804, https://doi.org/10.1016/j.engstruct.2011.06.004.

[15] Y. Shi, M. Su, L. Jiang, Q. Zhou, L. Guan, Y. Yang, L. Zhang, Seismic response analysis and connection performance evaluation of a hybrid coupled PEC wall system, Adv. Civil Eng. 2020 (2020) 8139697, https://doi.org/10.1155/2020/8139697.
[16] B. Tupper, Seismic Response of Reinforced Concrete Walls with Steel Boundary Elements, Master Thesis at the Department of Civil Engineering and Applied Mechanics, McGill University, Montreal, Canada, 1999.
[17] S. Tiwari, G. Mondal, S.R. Dash, K. Roy, Experimental investigation of unbonded reinforced concrete PT shear wall under lateral loading: a state-of-the-art review, J. Build. Eng. 78 (2023) 107504, https://doi.org/10.1016/j.jobe.2023.107504.
[18] K.M. Twigden, R.S. Henry, Snap back testing of unbonded post-tensioned concrete wall systems, Earthq. Struct. 16 (2) (2019) 209–2019, https://doi.org/10.12989/EAS.2019.16.2.209.
[19] M. Nazari, S. Sritharan, S. Aaleti, Single precast concrete rocking walls as earthquake force-resisting elements, Earthq. Eng. Struct. Dyn. 46 (5) (2017) 753–769, https://doi.org/10.1002/eqe.2829.
[20] M.J.N. Priestley, Overview of the PRESSS research program, PCI J. 36 (1991) 50–57.
[21] S. Pampanin, W.Y. Kam, G. Haverland, S. Gardiner, Expectation meets reality: seismic performance of a post-tensioned precast concrete building (PRESSS technology) during the 22nd Feb 2011 Christchurch Earthquake, in: New Zealand Concrete Industry Conference, New Zealand Concrete Society, Auckland, New Zealand, 2011.
[22] A. Cattanach, S. Pampanin, 21st century precast: the detailing and manufacture of NZ'S first multi-storey PRESSS-building, in: NZ Concrete Industry Conference, Rotorua, 2008.
[23] D. Kalliontzis, M. Morrison, Q. Liu, M. Nazari, V. Kotzamanis, Improving recovery of hybrid rocking walls through locally heat-treated replaceable bars for hysteretic energy dissipation, Eng. Struct. 267 (2022) 114621, https://doi.org/10.1016/j.engstruct.2022.114621.
[24] G. Xu, A. Li, Seismic performance and design approach of unbonded post-tensioned precast sandwich wall structures with friction devices, Eng. Struct. 204 (2020) 110037, https://doi.org/10.1016/j.engstruct.2019.110037.
[25] Y. Li, H. Zhang, H. Yu, J. An, Experimental study on seismic performance of a new self-centering coupling beam, J. Constr. Steel Res. 2016 (2024) 108572, https://doi.org/10.1016/j.jcsr.2024.108572.
[26] T. Guo, L. Wang, Z. Xu, Y. Hao, Experimental and numerical investigation of jointed self-centering concrete walls with friction connectors, Eng. Struct. 161 (2018) (2018) 192–206, https://doi.org/10.1016/j.engstruct.2018.02.028.
[27] H. Wu, J. Wang, L. Sui, T. Zhou, Y. Bai, Experimental investigation of self-centering steel reinforced concrete coupled wall panels with replaceable energy dissipaters, Eng. Struct. 212 (2020) (2020) 110473, https://doi.org/10.1016/j.engstruct.2020.110473.
[28] K.M. Twigden, S. Sritharan, R.S. Henry, Cyclic testing of unbonded post-tensioned concrete wall systems with and without supplemental damping, Eng. Struct. 140 (2017) (2017) 406–420, https://doi.org/10.1016/j.engstruct.2017.02.008.
[29] A. Astaneh-Asl, Seismic Behavior and Design of Composite Steel Plate Shear Walls, Report, Department of Civil and Environmental Engineering, University of California at Berkeley, May 2002.
[30] Q. Zhao, A. Astaneh-Asl, Cyclic behavior of traditional and innovative composite shear walls, J. Struct. Eng. 130 (2) (2004) 271–284, https://doi.org/10.1061/(ASCE)0733-9445130:2(271).
[31] T. Kang, Y. Qi, D. Chen, H. Wang, Q. Gu, Study on shear mechanism and design method of three-edges-connected composite plate shear wall partially infilling in steel frame, J. Build. Eng. 111 (2025) 113147, https://doi.org/10.1016/j.jobe.2025.113147.
[32] A. Dall'Asta, G. Leoni, A. Zona, B. Hoffmeister, H. Bigelow, H. Degée, C. Braham, T. Bogdan, W. Salvatore, F. Morelli, P. Tsintzos, S.A. Karamanos, G.E. Varelis, A. Galazzi, E. Medici, P. Boni, Innovative Hybrid and Composite Steel-Concrete Structural Solutions for Building in Seismic Area (INNO-HYCO), Grant Agreement RFSR-CT-2010-00025, 01/07/2010–30/06/2013, Final Report, Publications Office of the European Union, 2014, https://doi.org/10.2777/85404. ISBN 978-92-79-44080-9.
[33] A. Zona, H. Degée, G. Leoni, A. Dall'Asta, Ductile design of innovative steel and concrete hybrid coupled walls, J. Constr. Steel Res. 117 (2016) 204–213, https://doi.org/10.1016/j.jcsr.2015.10.017.
[34] R. Das, A. Zona, B. Vandoren, H. Degée, Optimizing the coupling ratio of seismic resistant HCW systems with shear links, J. Constr. Steel Res. 147 (2018) 393–407, https://doi.org/10.1016/j.jcsr.2018.04.026.
[35] R. Das, R. Steensels, D. Dragan, B. Vandoren, H. Degée, Characterization and optimization of a steel beam to RC wall connection for use in innovative hybrid coupled wall systems, Structures 23 (2020) 111–125, https://doi.org/10.1016/j.istruc.2019.10.011.
[36] F. Morelli, M. Manfredi, W. Salvatore, An enhanced component-based model for steel connection in a hybrid coupled shear wall structure: development, calibration and experimental validation, Comput. Struct. 176 (2016) (2016) 50–69, https://doi.org/10.1016/j.compstruc.2016.08.002.
[37] EN 1998-1, Eurocode 8: Design of Structures for Earthquake Resistance - Part 1: General Rules, Seismic Actions and Rules for Buildings, CEN, Brussels, 2026.
[38] FprEN 1998-1-2:2025-03, Eurocode 8: Design of Structures for Earthquake Resistance – Part 1–2: Earthquake Resistance Design of Structures, CEN, Brussels, 2026.
[39] FprEN 1998-1-1:2023-09, Eurocode 8: Earthquake Resistance Design of Structures – Part 1–1: General Rules and Seismic Action, CEN, Brussels, 2026.
[40] FprCEN /TS 1998-1-101:2025, Eurocode 8: Design of Structures for Earthquake Resistance – Part 1-101: Characterisation and Qualification of Structural Components for Seismic Applications by Means of Cyclic Tests, CEN/TC 250, 2026.
[41] ACI 318-25, Building Code for Structural Concrete - Code Requirements and Commentary, American Concrete Institute, Detroit, Michigan, 2025.
[42] ANSI/AISC 341-16, Seismic Provisions for Structural Steel Buildings, American Institute of Steel Construction, Chicago, Illinois, 2016.
[43] H. Degee, R. Das, A. Dall'Asta, A. Zona, F. Scozzese, W. Salvatore, F. Morelli, A. Natali, B. Hoffmeister, C. Vulcu, R. Mallardo, S. Karamanos, P. Tsintzos, G. Varelis, A. Galazzi, L. Bezzi, Innovative Steel-Concrete HYbrid Coupled Walls for Buildings in Seis-Mic Areas: Advancements and Design Guidelines – HYCAD, 2020-2023. RFCS project: GA No. 899381.
[44] ECCS, Recommended Testing Procedure for Assessing the Behaviour of Structural Steel Elements under Cyclic Load, 1986. TC 1, TWG 1.3.
[45] CEN, EN 15129, Anti-seismic devices, European Committee for Standardization, Brussels, 2010.
[46] C. Vulcu, B. Hoffmeister, A. Natali, F. Morelli, Deliverable 3.3 - Report on the results of the experimental tests, in: Innovative Steel-Concrete HYbrid Coupled Walls for Buildings in Seismic Areas: Advancements and Design Guidelines – HYCAD, 2026. RFCS project: GA No. 899381.
[47] C. Vulcu, B. Hoffmeister, R. Das, H. Degee, HCWs with replaceable shear links: experimental input and seismic performance of a multi-story building, in: F. M. Mazzolani, V. Piluso, E. Nastri, A. Formisano (Eds.), Proceedings of the 11th International Conference on Behaviour of Steel Structures in Seismic Areas. STESSA 2024, Lecture Notes in Civil Engineering, vol. 519, Springer, Cham, 2024, https://doi.org/10.1007/978-3-031-62884-9_85.
[48] Z. Qu, A. Wada, S. Motoyui, H. Sakata, S. Kishiki, Pin-supported walls for enhancing the seismic performance of building structures, Earthq. Eng. Struct. Dyn. 41 (2012) 2075–2091, https://doi.org/10.1002/eqe.2175.
[49] A. Ioan, A. Stratan, D. Dubină, M. Poljanšek, F.J. Molina, F. Taucer, P. Pegon, G. Sabău, Experimental validation of re-centring capability of eccentrically braced frames with removable links, Eng. Struct. 113 (2016) 335–346. ISSN 0141-0296, https://doi.org/10.1016/j.engstruct.2016.01.038.
[50] R. Das, et al., Seismic behaviour of an innovative hybrid coupled wall system investigated through cyclic tests, in: F.M. Mazzolani, V. Piluso, E. Nastri, A. Formisano (Eds.), Proceedings of the 11th International Conference on Behaviour of Steel Structures in Seismic Areas. STESSA 2024, Lecture Notes in Civil Engineering, vol. 520, Springer, Cham, 2024, https://doi.org/10.1007/978-3-031-62888-7_6.